## On the Dynamics and Control of Flexible Multibody Systems with Closed Loops


Christopher J. Damaren



*The International Journal of Robotics Research* 2000 19: 238
DOI: 10.1177/02783640022066842

**Christopher J. Damaren**

University of Toronto
Institute for Aerospace Studies
4925 Dufferin Street
Toronto, Ontario M3H 5T6, Canada

# On the Dynamics and Control of Flexible Multibody Systems with Closed Loops

## Abstract

*The motion control problem for cooperating flexible robot arms manipulating a large rigid payload is considered. An output that depends on the payload position and contributions from the joint motion of each arm is constructed whose rate yields the passivity property with respect to a special input. The input is a combination of the torques from each arm and contains a free load-sharing parameter. The passivity property is shown to depend on the payload mass properties, and in cases where the payload is large, a passivity-based controller combining feedforward and feedback as elements is devised, which yields tracking. An experimental facility consisting of two planar 3-DoF arms is used to implement the strategies. Good tracking is observed and compared with simulation predictions for closed-loop flexible multibody systems.*

KEY WORDS—cooperating robots, flexible manipulators, trajectory control

## 1. Introduction

The problem of cooperating robot arms has attracted much attention within the robotics community. Multiple arms have many advantages, including increased payload capacity because of the redundant actuation and stiffer structure. Lightweight arms such as those being developed for the Space Station introduce the added complexity of structural flexibility. However, the additional compliance can be beneficial. Possible disadvantages include a reduction in the robot workspace. Motivated by space scenarios, this paper addresses the motion control problem associated with the manipulation of large payloads by two lightweight flexible arms. An overview of the control problem for flexible robot manipulators in a chain topology is presented by Book (1993) and Canudas de Wit, Siciliano, and Bastin (1996).

The International Journal of Robotics Research
Vol. 19, No. 3, March 2000, pp. 238-253,


Cooperating robot systems contain a topological closed loop, which complicates the dynamics and control problem. In the case where the links are rigid bodies, several procedures have evolved for solving the forward dynamics problem. One broad class of methods expresses the motion in terms of the null basis associated with a homogeneous velocity constraint (Garcia de Jalon and Bayo 1994). This technique will be used here in conjunction with the linearized motion equations to characterize the closed-loop modal characteristics.

Another method for the simulation dynamics decomposes the accelerations into a free component associated with the equivalent cut-chain and a closed-loop component chosen to the satisfy the loop closure constraint (Lilly and Orin 1991). This method has been applied to rigid loops mounted on a free spacecraft (Bonaventura and Lilly 1995) and will be used here to extend our previous simulation capability for flexible multibody chains (Damaren and Sharf 1995) to deal with the closed-loop case. The simulation of two planar cooperating flexible arms has been considered by Krishnamurthy and Yang (1995) who treated a system similar to the experimental rig considered here.

The inverse dynamics problem for rigid closed-loop systems was efficiently solved by Nakamura and Ghodoussi (1989) who showed how the torques required could be obtained from those of the equivalent cut-loop system. They also showed how the potentially overactuated nature of these systems could be used to optimize the torque demand. In subsequent work, the inverse dynamics solution formed the basis for a computed torque solution of the control problem (Uecker, Wang, and Kokkinis 1991). Other contributions to the control problem for cooperating rigid arms are summarized by Uchiyama (1998) and Unseren (1998) who emphasize the simultaneous control of payload position and internal forces. Modeling and control issues for flexible arms in contact with the environment are discussed by Hu and Ulsoy (1994) and Yim and Singh (1995).

The passivity property of mechanical systems with collocated force (torque) actuators and rate (angular rate)

outputs has played an important role in the development of robot controllers (Ortega et al. 1998). In structurally flexible systems, the controlled output is the payload motion that is noncollocated and typically leads to nonminimum phase, hence nonpassive, input-output behavior. The origins of our work can be traced to Wang and Vidyasagar (1990, 1991) who showed that a modified output (the reflected tip rate) could yield passivity for a single flexible link. In the multilink case, we have developed an output that combined joint motions and tip (payload) motions so as to realize a passive mapping from (inverse transpose of Jacobian multiplied by) joint torques to the modified output rate (Damaren 1995). The use of a strictly passive feedback with this output leads to endpoint stabilization as well as simultaneous vibration suppression. A feedforward torque, which preserved passivity in the error dynamics, was presented in (Damaren 1996a), and an adaptive form was explored in (Damaren 1996b). These works relied on the payload being much more massive than the arm. Damaren (1998) extended the approach to situations where the stator mass at each joint could be large as well.

In this paper, the passivity-based approach is extended to the situation where two flexible arms manipulate a large common rigid object. A set of inputs and outputs is introduced, which leads to the passivity property in situations mirroring those of the corresponding chain topology. These variables contain a free load-sharing parameter that permits the designer to share the required torque between each arm in a largely arbitrary fashion. An experimental facility consisting of two planar arms with three joints each and flexible links is described in the paper and used to implement the proposed controllers. The experimental results confirm the theoretical ideas.

## 2. Dynamics of Flexible Multibody Loops

Consider a chain of flexible and/or rigid bodies $\{\mathcal{B}_0, \mathcal{B}_1, \mathcal{B}_2, \cdots, \mathcal{B}_N\}$ with bodies $\mathcal{B}_0$ and $\mathcal{B}_N$ cantilevered in an inertial reference frame $\mathcal{F}_0$ so as to form a closed loop (Fig. 1). The bodies are connected by revolute joints, and $\boldsymbol{\theta} = \text{col}\{\theta_n\}$, $n = 1 \cdots N$ denotes the collection of joint angles and $\mathbf{q}_e = \text{col}\{\mathbf{q}_{en}\}$ is the collection of $N_e$ elastic degrees of freedom. It is assumed that these are generated using cantilevered boundary conditions for the elastic deflections at the inboard end of each body. The collection of generalized coordinates can be written as $\mathbf{q} = \text{col}\{\boldsymbol{\theta}, \mathbf{q}_e\}$.

The Cartesian displacement of $\mathcal{B}_n$ relative to $\mathcal{F}_0$ is written as $\boldsymbol{\rho}_n$, which is interpreted as a sextuple whose top half contains the position coordinates and whose bottom half is the orientation parameterized by an integrable attitude representation, i.e., Euler angles. Since $\mathcal{B}_N$ is fixed, the appropriate kinematical constraint can be written as

$$\dot{\boldsymbol{\rho}}_N = \mathbf{J}_c(\mathbf{q})\dot{\mathbf{q}} = \mathbf{0}, \tag{1}$$

where $\mathbf{J}_c$ is the appropriate Jacobian matrix.

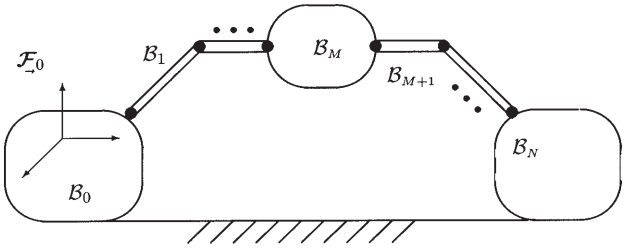


Fig. 1. Closed-loop multibody system.

The motion equation for the flexible closed loop (omitting structural damping) can be written as

$$\mathbf{M}(\mathbf{q})\ddot{\mathbf{q}} + \mathbf{K}\mathbf{q} = [\mathbf{1}\ \ \mathbf{O}]^T\boldsymbol{\tau} + \mathbf{f}_{non}(\mathbf{q}, \dot{\mathbf{q}}) + \mathbf{J}_c^T\boldsymbol{\lambda}, \tag{2}$$

subject to the constraint in (1). $\mathbf{M}$, $\mathbf{K}$, and $\boldsymbol{\tau}$ are the mass matrix, stiffness matrix, and joint torques, respectively, and the nonlinear inertial forces $\mathbf{f}_{non}$ are quadratic in $\dot{\mathbf{q}}$. These matrices can be partitioned consistent with $\mathbf{q}$:

$$\mathbf{M} = \begin{bmatrix} \mathbf{M}_{\theta\theta} & \mathbf{M}_{\theta e} \\ \mathbf{M}_{\theta e}^T & \mathbf{M}_{ee} \end{bmatrix}, \quad \mathbf{K} = \begin{bmatrix} \mathbf{O} & \mathbf{O} \\ \mathbf{O} & \mathbf{K}_{ee} \end{bmatrix}, \tag{3}$$

with $\mathbf{M} = \mathbf{M}^T > \mathbf{O}$ and $\mathbf{K}_{ee} = \mathbf{K}_{ee}^T > \mathbf{O}$. The constraint forces required to enforce (1) are given by $\boldsymbol{\lambda}$, and with $\boldsymbol{\lambda} = \mathbf{0}$, (2) is equivalent to the motion equation for the equivalent chain where $\mathcal{B}_N$ is free to move.

The body $\mathcal{B}_M$, $1 \le M \le N$ is taken to be a rigid payload under manipulation, and it is assumed that $M$ is equal to the number of rigid degrees of freedom after loop closure. The system can be interpreted as two arms cooperatively manipulating the payload $\mathcal{B}_M$. To this end, the joint angles and elastic coordinates are further partitioned as

$$\begin{aligned} \boldsymbol{\theta}_1 &= \text{col}\{\theta_n\}, n = 1, \cdots, M, \\ \boldsymbol{\theta}_2 &= \text{col}\{\theta_n\}, n = M+1, \cdots, N \end{aligned} \tag{4}$$

$$\begin{aligned} \mathbf{q}_{1e} &= \text{col}\{\mathbf{q}_{en}\}, n = 1, \cdots, M, \\ \mathbf{q}_{2e} &= \text{col}\{\mathbf{q}_{en}\}, n = M+1, \cdots N. \end{aligned} \tag{5}$$

The payload position can be summarized by two forms of the forward kinematics map: $\boldsymbol{\rho} = \mathcal{F}_1(\boldsymbol{\theta}_1, \mathbf{q}_{e1}) = \mathcal{F}_2(\boldsymbol{\theta}_2, \mathbf{q}_{e2})$, where, for simplicity, we write $\boldsymbol{\rho} \equiv \boldsymbol{\rho}_M$. Hence, the payload velocity can be written as

$$\begin{aligned} \dot{\boldsymbol{\rho}} &= \mathbf{J}_{1\theta}(\boldsymbol{\theta}_1, \mathbf{q}_{1e})\dot{\boldsymbol{\theta}}_1 + \mathbf{J}_{1e}(\boldsymbol{\theta}_1, \mathbf{q}_{1e})\dot{\mathbf{q}}_{1e} \\ &= \mathbf{J}_{2\theta}(\boldsymbol{\theta}_2, \mathbf{q}_{2e})\dot{\boldsymbol{\theta}}_2 + \mathbf{J}_{2e}(\boldsymbol{\theta}_2, \mathbf{q}_{2e})\dot{\mathbf{q}}_{2e}, \end{aligned} \tag{6}$$

where $\mathbf{J}_{i\theta}$, $\mathbf{J}_{ie}$, $i = 1, 2$, are the required Jacobian matrices. It will be assumed that $\mathbf{J}_{1\theta}$ is invertible.

An output of fundamental importance in the sequel is the $\mu$-tip rate defined by

$$\begin{aligned} \dot{\boldsymbol{\rho}}_\mu &= C_1[\mathbf{J}_{1\theta}\dot{\boldsymbol{\theta}}_1 + \mu\mathbf{J}_{1e}\dot{\mathbf{q}}_{1e}] + C_2[\mathbf{J}_{2\theta}\dot{\boldsymbol{\theta}}_2 + \mu\mathbf{J}_{2e}\dot{\mathbf{q}}_{2e}] \quad (7) \\ &= \dot{\boldsymbol{\rho}} - (1-\mu)[C_1\mathbf{J}_{1e}\dot{\mathbf{q}}_{1e} + C_2\mathbf{J}_{2e}\dot{\mathbf{q}}_{2e}] \\ &= \mu\dot{\boldsymbol{\rho}} + (1-\mu)[C_1\mathbf{J}_{1\theta}\dot{\boldsymbol{\theta}}_1 + C_2\mathbf{J}_{2\theta}\dot{\boldsymbol{\theta}}_2], \quad (8) \end{aligned}$$

where $C_1$ with $0 < C_1 < 1$ and $C_2 = 1 - C_1$ will be termed *load-sharing parameters*. For $\mu = 1$, $\boldsymbol{\rho}_\mu = \boldsymbol{\rho}$, the true payload position, while for $\mu = 0$, $\boldsymbol{\rho}_\mu$ describes an output based on the joint motion alone. If the approximations $\mathbf{J}_{i\theta}(\boldsymbol{\theta}_i, \mathbf{q}_{ie}) \doteq \mathbf{J}_{i\theta}(\boldsymbol{\theta}_i, \mathbf{0})$, $i = 1, 2$, are made, then the integral of (8) yields

$$\boldsymbol{\rho}_\mu(t) = \mu\boldsymbol{\rho}(t) + (1-\mu)[C_1\mathcal{F}_1(\boldsymbol{\theta}_1, \mathbf{0}) + C_2\mathcal{F}_2(\boldsymbol{\theta}_2, \mathbf{0})], \tag{9}$$

where $\mathcal{F}_i(\boldsymbol{\theta}_i, \mathbf{0})$ are the rigid forward kinematical maps. If one arm is rigid, say $i = 1$, then $\boldsymbol{\rho} = \mathcal{F}_1(\boldsymbol{\theta}_1, \mathbf{0})$ and $\boldsymbol{\rho}_\mu$ can be constructed from joint measurements alone.

### *2.1. Forward Dynamics*

There are several established techniques for solving the motion equations (2) for the accelerations $\ddot{\mathbf{q}}$ subject to the constraint (1). One uses a suitable decomposition for the accelerations, while the other describes the null-space of $\mathbf{J}_c$.

In the first method, the acceleration is written as $\ddot{\mathbf{q}} = \ddot{\mathbf{q}}_{op} + \ddot{\mathbf{q}}_{cl}$, where the "open-loop" part $\ddot{\mathbf{q}}_{op}$ is the solution of (2) with $\boldsymbol{\lambda} = \mathbf{0}$. It represents the accelerations of the corresponding open chain. The correction $\ddot{\mathbf{q}}_{cl}$ is the solution of

$$\ddot{\mathbf{q}}_{cl} = \mathbf{M}^{-1}\mathbf{J}_c^T\boldsymbol{\lambda}, \tag{10}$$

which follows from substituting the assumed expression for $\ddot{\mathbf{q}}$ into the motion equation. The constraint forces are determined so that

$$\ddot{\boldsymbol{\rho}}_N = \mathbf{J}_c(\ddot{\mathbf{q}}_{op} + \ddot{\mathbf{q}}_{cl}) + \dot{\mathbf{J}}_c\dot{\mathbf{q}} = \mathbf{J}_c\ddot{\mathbf{q}}_{cl} + \ddot{\boldsymbol{\rho}}_{op} = \mathbf{0}, \tag{11}$$

where $\ddot{\boldsymbol{\rho}}_{op}$ is the "tip" acceleration calculated using $\ddot{\mathbf{q}}_{op}$ and the current state of the system. It follows from substituting $\ddot{\mathbf{q}}_{cl}$ from (10) into (11) so that

$$\boldsymbol{\lambda} = -\boldsymbol{\Lambda}\ddot{\boldsymbol{\rho}}_{op}, \quad \boldsymbol{\Lambda} \triangleq (\mathbf{J}_c\mathbf{M}^{-1}\mathbf{J}_c^T)^{-1}, \tag{12}$$

and hence $\ddot{\mathbf{q}} = \ddot{\mathbf{q}}_{op} - \mathbf{M}^{-1}\mathbf{J}_c^T\boldsymbol{\Lambda}\ddot{\boldsymbol{\rho}}_{op}$. The advantage of this approach is that recursive algorithms suitable for the open-chain case can be used to determine $\ddot{\mathbf{q}}_{op}$. Furthermore, the matrix $\mathbf{M}^{-1}$ and the constraint Jacobian can also be calculated recursively. The algorithms used here are presented by Damaren and D'Eleuterio (1989), and the implementation for flexible chains is comprehensively discussed by Damaren and Sharf (1995). This approach will form the basis of our simulation results in Section 6. However, despite its computational efficiency and suitability for simulation, it is not a useful description for control system design.

With the second method, we determine the matrix $\mathbf{R}(\mathbf{q})$ such that $\mathbf{J}_c\mathbf{R} = \mathbf{O}$ and then expand the solution as

$$\dot{\mathbf{q}} = \mathbf{R}(\mathbf{q})\dot{\mathbf{z}}, \tag{13}$$

which automatically satisfies the constraint (1). Rather than take $\mathbf{J}_c$ as $\partial\boldsymbol{\rho}_N/\partial\mathbf{q}^T$, another possible choice for the constraint Jacobian is

$$\mathbf{J}_c = [\mathbf{J}_{1\theta} \quad -\mathbf{J}_{2\theta} \quad \mathbf{J}_{1e} \quad -\mathbf{J}_{2e}], \tag{14}$$

which also enforces loop closure. Partitioning the independent coordinates $\mathbf{z} = \text{col}\{\mathbf{z}_r, \mathbf{z}_e\}$, the null basis can be written as

$$\mathbf{R} = \begin{bmatrix} \mathbf{R}_{\theta r} & \mathbf{R}_{\theta e} \\ \mathbf{R}_{er} & \mathbf{R}_{ee} \end{bmatrix}. \tag{15}$$

Since $\mathbf{R}$ can always be postmultiplied by a square invertible matrix, we can without loss in generality select $\mathbf{z}_r = \boldsymbol{\theta}_1$ and $\mathbf{z}_e = \mathbf{q}_e$ so that

$$\begin{aligned} \mathbf{R}_{\theta r} &= \begin{bmatrix} \mathbf{1} \\ \widehat{\mathbf{R}}_{\theta r} \end{bmatrix}, \quad \mathbf{R}_{\theta e} = \begin{bmatrix} \mathbf{O} \\ \widehat{\mathbf{R}}_{\theta e} \end{bmatrix}, \\ \widehat{\mathbf{R}}_{\theta e} &= [\widehat{\mathbf{R}}_{\theta e,1} \quad \widehat{\mathbf{R}}_{\theta e,2}] \\ \mathbf{R}_{er} &= \mathbf{O}, \qquad \mathbf{R}_{ee} = \mathbf{1}. \end{aligned} \tag{16}$$

Given these descriptions, the original Jacobian matrices are connected by

$$\mathbf{J}_{1\theta} = \mathbf{J}_{2\theta}\widehat{\mathbf{R}}_{\theta r}, \quad \mathbf{J}_{1e} = \mathbf{J}_{2\theta}\widehat{\mathbf{R}}_{\theta e,1}, \quad \mathbf{J}_{2e} = -\mathbf{J}_{2\theta}\widehat{\mathbf{R}}_{\theta e,2}. \tag{17}$$

Substituting (13) into (2) and premultiplication by $\mathbf{R}^T$ yields

$$\begin{aligned} \mathbf{M}_{zz}(\mathbf{q})\ddot{\mathbf{z}} + \mathbf{K}_{zz}\mathbf{z} &= \mathbf{R}^T[\mathbf{1} \quad \mathbf{O}]^T\boldsymbol{\tau} \\ &\quad + \mathbf{R}^T[\mathbf{f}_{non}(\mathbf{q}, \dot{\mathbf{q}}) - \mathbf{M}\dot{\mathbf{R}}\dot{\mathbf{z}}], \end{aligned} \tag{18}$$

where the constraint vector has been eliminated on account of the property relating $\mathbf{J}$ and $\mathbf{R}$, and

$$\mathbf{M}_{zz} = \mathbf{R}^T\mathbf{M}\mathbf{R}, \quad \mathbf{K}_{zz} = \mathbf{R}^T\mathbf{K}\mathbf{R}. \tag{19}$$

The reader may verify that relative to $\mathbf{z}$, the reduced mass and stiffness matrices take the forms

$$\mathbf{M}_{zz} = \begin{bmatrix} \mathbf{M}_{zz,rr} & \mathbf{M}_{zz,re} \\ \mathbf{M}_{zz,re}^T & \mathbf{M}_{zz,ee} \end{bmatrix}, \quad \mathbf{K}_{zz} = \begin{bmatrix} \mathbf{O} & \mathbf{O} \\ \mathbf{O} & \mathbf{K}_{ee} \end{bmatrix}, \tag{20}$$

where $\mathbf{M}_{zz,rr} = \mathbf{R}_{\theta r}^T\mathbf{M}_{\theta\theta}\mathbf{R}_{\theta r}$, $\mathbf{M}_{zz,re} = \mathbf{R}_{\theta r}^T[\mathbf{M}_{\theta\theta}\mathbf{R}_{\theta e} + \mathbf{M}_{\theta e}]$.

## 3. Modal Analysis

Now consider small excursions of the coordinates, $\delta\mathbf{z} = \mathbf{R}(\bar{\mathbf{q}})\delta\mathbf{q}$, in the vicinity of a constant configuration $\bar{\mathbf{q}} = \text{col}\{\bar{\boldsymbol{\theta}}, \mathbf{0}\}$. In this case, $\mathbf{R}(\bar{\mathbf{q}})$ can be effectively calculated from the singular value decomposition of $\mathbf{J}_c(\bar{\mathbf{q}})$ by forming its columns from the right singular vectors corresponding to

the $N + N_e - M$ zero singular values. It must be postmultiplied by a square invertible transformation chosen to yield the forms in (16). The linearized form of eq. (18) is

$$\mathbf{M}_{zz}(\bar{\mathbf{q}})\delta\ddot{\mathbf{z}} + \mathbf{K}_{zz}\delta\mathbf{z} = \mathbf{B}(\bar{\mathbf{q}})\boldsymbol{\tau}, \quad \mathbf{B}^T = [\mathbf{R}_{\theta r} \;\; \mathbf{R}_{\theta e}], \tag{21}$$

and the corresponding eigenproblem can be written as

$$-\omega_\alpha^2\mathbf{M}_{zz}(\bar{\mathbf{q}})\mathbf{z}_\alpha + \mathbf{K}\mathbf{z}_\alpha = \mathbf{0}, \tag{22}$$

where $\omega_\alpha$ are the unconstrained (joints unlocked) vibration frequencies and $\mathbf{q}_\alpha = \text{col}\{\boldsymbol{\theta}_\alpha, \mathbf{q}_{e\alpha}\} = \mathbf{R}(\bar{\mathbf{q}})\mathbf{z}_\alpha$, $\alpha = 1 \cdots N_e$, are the eigenvectors (mode shapes). Note that $\boldsymbol{\theta}_\alpha$ are the mode slopes at each joint axis and it is assumed that $\boldsymbol{\theta}_\alpha$ and $\mathbf{q}_{e\alpha}$ can be further partitioned as in (4) and (5). Given the assumptions, there are also $M$ zero-frequency rigid modes collectively of the form $\mathbf{Z}_r = [\mathbf{1} \;\; \mathbf{O}]^T$. The modes satisfy standard orthonormality relations with respect to $\mathbf{M}_{zz}$ and $\mathbf{K}_{zz}$:

$$\mathbf{z}_\alpha^T\mathbf{M}_{zz}\mathbf{z}_\beta = \delta_{\alpha\beta}, \qquad \mathbf{z}_\alpha^T\mathbf{M}_{zz}\mathbf{Z}_r = \mathbf{O}, \tag{23}$$

$$\mathbf{z}_\alpha^T\mathbf{K}_{zz}\mathbf{z}_\beta = \omega_\alpha^2\delta_{\alpha\beta}, \quad \mathbf{z}_\alpha^T\mathbf{K}_{zz}\mathbf{Z}_r = \mathbf{O}, \quad \alpha, \beta = 1 \cdots N_e. \tag{24}$$

Expanding the solution of eq. (21) in terms of eigenvectors, $\delta\mathbf{z}(t) = \mathbf{Z}_r\boldsymbol{\eta}_r(t) + \sum_\alpha \mathbf{z}_\alpha\eta_\alpha(t)$, it is relatively straightforward to obtain the modal equations

$$\mathbf{M}_{zz,rr}\ddot{\boldsymbol{\eta}}_r = \mathbf{R}_{\theta r}^T\boldsymbol{\tau}(t), \quad \ddot{\eta}_\alpha + \omega_\alpha^2\eta_\alpha = \boldsymbol{\theta}_\alpha^T\boldsymbol{\tau}\ , \quad \alpha = 1 \cdots N_e. \tag{25}$$

The modal expansion for $\delta\mathbf{z}$ is equivalent to $\delta\boldsymbol{\theta} = \mathbf{R}_{\theta r}\boldsymbol{\eta}_r + \sum_\alpha[\boldsymbol{\theta}_{1\alpha}^T \;\; \boldsymbol{\theta}_{2\alpha}^T]^T\eta_\alpha$ and $\delta\mathbf{q}_e = \sum_\alpha[\mathbf{q}_{1e\alpha}^T \;\; \mathbf{q}_{2e\alpha}^T]^T\eta_\alpha$. Linearizing the expansion for the $\mu$-tip rate in (7) and substituting the modal expansion gives

$$\dot{\boldsymbol{\rho}}_\mu = (C_1\mathbf{J}_{1\theta} + C_2\mathbf{J}_{2\theta}\widehat{\mathbf{R}}_{\theta r})\dot{\boldsymbol{\eta}}_r + \sum_{\alpha=1}^{N_e}\mathbf{c}_\alpha\dot{\eta}_\alpha, \tag{26}$$

$$\mathbf{c}_\alpha \triangleq C_1(\mathbf{J}_{1\theta}\boldsymbol{\theta}_{1\alpha} + \mu\mathbf{J}_{1e}\mathbf{q}_{1e\alpha}) + C_2(\mathbf{J}_{2\theta}\boldsymbol{\theta}_{2\alpha} + \mu\mathbf{J}_{2e}\mathbf{q}_{2e\alpha}), \tag{27}$$

where all Jacobian matrices are evaluated at the reference condition. Now assume that the torques are determined according to

$$\boldsymbol{\tau} = [C_1\mathbf{J}_{1\theta} \quad C_2\mathbf{J}_{2\theta}]^T\widehat{\boldsymbol{\tau}}, \tag{28}$$

where $\widehat{\boldsymbol{\tau}}$ is a collection of $M$ control inputs. This motivates the term load-sharing parameter for the $C_i$.

Using Laplace transforms in conjunction with (25) through (28), while noting that $\mathbf{J}_{2\theta}\widehat{\mathbf{R}}_{\theta r} = \mathbf{J}_{1\theta}$ and $C_1 + C_2 = 1$, the dynamics of the linearized system relating $\widehat{\boldsymbol{\tau}}$ to $\dot{\boldsymbol{\rho}}_\mu$ can be captured by the input-output description:

$$\begin{aligned}\dot{\boldsymbol{\rho}}_\mu(s) &= \mathbf{G}(s)\widehat{\boldsymbol{\tau}}(s),\\ \mathbf{G}(s) &= \frac{1}{s}\mathbf{J}_{1\theta}\mathbf{M}_{zz,rr}^{-1}\mathbf{J}_{1\theta}^T + \sum_{\alpha=1}^{N_e}\frac{s}{s^2+\omega_\alpha^2}\mathbf{c}_\alpha\mathbf{b}_\alpha^T, \quad (29)\\ \mathbf{b}_\alpha &= C_1\mathbf{J}_{1\theta}\boldsymbol{\theta}_{1\alpha} + C_2\mathbf{J}_{2\theta}\boldsymbol{\theta}_{2\alpha}. \quad (30)\end{aligned}$$

The system in (29) is passive if $\int_0^T \dot{\boldsymbol{\rho}}_\mu^T\widehat{\boldsymbol{\tau}}\,dt \geq 0$, $\forall T \geq 0$, and $\forall\widehat{\boldsymbol{\tau}}$ such that $\int_0^T \widehat{\boldsymbol{\tau}}^T\widehat{\boldsymbol{\tau}}\,dt < \infty$. For linear time-invariant systems, this is equivalent to positive realness of the corresponding transfer function $\mathbf{G}(s)$, i.e., $\mathbf{G}(s)$ is analytic and $\mathbf{G}(s) + \mathbf{G}^H(s) \geq \mathbf{O}$ for $s$ in the open right-half plane. Since $1/s$ and $s/(s^2+\omega_\alpha^2)$ are positive real, $\mathbf{G}(s)$ in (29) is positive real if and only if $\mathbf{J}_{1\theta}\mathbf{M}_{zz,rr}^{-1}\mathbf{J}_{1\theta}^T$ and $\mathbf{c}_\alpha\mathbf{b}_\alpha^T$ are symmetric and positive-semidefinite (Newcomb, 1966). Clearly this is true for the rigid contribution. The easiest way for $\mathbf{c}_\alpha\mathbf{b}_\alpha^T \geq \mathbf{O}$ is $\mathbf{c}_\alpha = \mathbf{b}_\alpha$, which occurs for $\mu = 0$; then, $\dot{\boldsymbol{\rho}}_\mu$ depends only on the joint motion. The next section seeks to enlarge the range of $\mu$ leading to passivity, thus introducing the payload motion $\dot{\boldsymbol{\rho}}$ into $\dot{\boldsymbol{\rho}}_\mu$ according to (8).

## 4. Linear Passivity Analysis for Flexible Closed Loops

Let us define the modal amplitude at the payload according to

$$\boldsymbol{\rho}_\alpha \triangleq \mathbf{J}_{1\theta}\boldsymbol{\theta}_{1\alpha} + \mathbf{J}_{1e}\mathbf{q}_{1e\alpha} = \mathbf{J}_{2\theta}\boldsymbol{\theta}_{2\alpha} + \mathbf{J}_{2e}\mathbf{q}_{2e\alpha}. \tag{31}$$

LEMMA 1. If $\boldsymbol{\rho}_\alpha = \mathbf{0}$, $\alpha = 1 \cdots N_e$, i.e., all vibration modes exhibit a node at the payload, then $\mathbf{G}(s)$ in (29) is positive real for $\mu < 1$.

**Proof.** From (31), $\mathbf{J}_{ie}\mathbf{q}_{ie,\alpha} = -\mathbf{J}_{i\theta}\boldsymbol{\theta}_{i\alpha}$, $i = 1, 2$, so that $\mathbf{c}_\alpha = (1-\mu)\mathbf{b}_\alpha$. Hence from (29),

$$\mathbf{G}(s) = \frac{1}{s}\mathbf{J}_{1\theta}\mathbf{M}_{zz,rr}^{-1}\mathbf{J}_{1\theta}^T + \sum_{\alpha=1}^{N_e}\frac{s}{s^2+\omega_\alpha^2}(1-\mu)\mathbf{b}_\alpha\mathbf{b}_\alpha^T, \tag{32}$$

which is positive real for $\mu < 1$. □

Note that controllability and observability of each mode depends on $\mathbf{c}_\alpha\mathbf{b}_\alpha^T \neq \mathbf{0}$ necessitating $\mu < 1$. We also disallow $C_1 = 0$ and $C_2 = 0$ since localization of a vibration mode within a single arm ($\boldsymbol{\theta}_{1\alpha} = \mathbf{0}$ or $\boldsymbol{\theta}_{2\alpha} = \mathbf{0}$) leads to $\mathbf{c}_\alpha\mathbf{b}_\alpha^T = \mathbf{0}$ in one of these cases according to (30). It is also clear from the form of eq. (32) that a PD feedback applied to $\boldsymbol{\rho}_\mu$ leads to active damping of the vibration modes in addition to control of the rigid body mode. This is possible for $\mu = 0$, but the tip position no longer appears in the measurement.

In Damaren (1998), a necessary and sufficient condition for $\boldsymbol{\rho}_\alpha = \mathbf{0}$, $\alpha = 1 \cdots N_e$, was uncovered for a flexible multibody chain manipulating a payload at its tip:

$$\mathbf{M}_{\theta\theta}\mathbf{J}_\theta^{-1}\mathbf{J}_e = \mathbf{M}_{\theta e}. \tag{33}$$

This was shown to be closely achievable for large payloads in general and, with or without large stator masses at the end of each link, for planar two- and three-link arms. The corresponding result for the closed-loop system is given below.

LEMMA 2. The mode shapes, $\mathbf{q}_\alpha = \mathbf{R}\mathbf{z}_\alpha$, of (22) satisfy $\boldsymbol{\rho}_\alpha \triangleq \mathbf{0}$, $\alpha = 1 \cdots N_e$, if and only if

$$\mathbf{M}_{zz,rr}\mathbf{J}_{1\theta}^{-1}\widehat{\mathbf{J}}_{e1} = \mathbf{M}_{zz,re}, \tag{34}$$

where $\widehat{\mathbf{J}}_{e1} = [\mathbf{J}_{e1} \;\; \mathbf{O}]$.

**Proof.** Using the eigenequation (22) and the partitioning of the mass and stiffness matrices in (2), the eigencolumns satisfy $\mathbf{M}_{zz,rr}\mathbf{z}_{r\alpha} + \mathbf{M}_{zz,re}\mathbf{z}_{e\alpha} = \mathbf{0}$. Thus,

$$\begin{aligned}\mathbf{J}_{1\theta}\boldsymbol{\theta}_{1\alpha} + \mathbf{J}_{1e}\mathbf{q}_{1e\alpha} &= \mathbf{J}_{1\theta}(\mathbf{z}_{r\alpha} + \mathbf{J}_{1\theta}^{-1}\widehat{\mathbf{J}}_{1e})\mathbf{z}_{e\alpha} \\ &= \mathbf{J}_{1\theta}\mathbf{M}_{zz,rr}^{-1}(\mathbf{M}_{zz,rr}\mathbf{J}_{1\theta}^{-1}\widehat{\mathbf{J}}_{e1} - \mathbf{M}_{zz,re})\mathbf{z}_{e\alpha}.\end{aligned}$$

Clearly, we have sufficiency. Now, suppose that $\boldsymbol{\rho}_\alpha = \mathbf{0}$. Since the $N_e$ $\mathbf{z}_{e\alpha} = \mathbf{q}_{e\alpha}$ are linearly independent, the null space of the $M \times N_e$ matrix $(\mathbf{M}_{zz,rr}\mathbf{J}_{1\theta}^{-1}\widehat{\mathbf{J}}_{e1} - \mathbf{M}_{zz,re})$ must have dimension $N_e$; hence $\mathbf{M}_{zz,rr}\mathbf{J}_{1\theta}^{-1}\widehat{\mathbf{J}}_{e1} - \mathbf{M}_{zz,re} = \mathbf{O}$. □

It is now shown that the property in Lemma 2 is closely achieved for large payloads. Decompose the mass matrix into

$$\mathbf{M} = \delta\mathbf{M} + [\mathbf{J}_{1\theta} \;\; \mathbf{O} \;\; \mathbf{J}_{1e} \;\; \mathbf{O}]^T\mathbf{M}_P[\mathbf{J}_{1\theta} \;\; \mathbf{O} \;\; \mathbf{J}_{1e} \;\; \mathbf{O}], \tag{35}$$

where $\mathbf{M}_P$ is the payload contribution and $\delta\mathbf{M}$ denotes the remainder. Correspondingly, using (20) *et seq.*, (16), and (17),

$$\begin{aligned}\mathbf{M}_{zz,rr} &= \delta\mathbf{M}_{zz,rr} + \mathbf{R}_{\theta r}^T[\mathbf{J}_{1\theta}\mathbf{O}]^T\mathbf{M}_P[\mathbf{J}_{1\theta}\mathbf{O}]\mathbf{R}_{\theta r} \\ &\doteq \mathbf{J}_{1\theta}^T\mathbf{M}_P\mathbf{J}_{1\theta} \qquad (36)\\ \mathbf{M}_{zz,re} &= \delta\mathbf{M}_{zz,re} + \mathbf{R}_{\theta r}^T[\mathbf{J}_{1\theta}\mathbf{O}]^T\mathbf{M}_P([\mathbf{J}_{1\theta}\mathbf{O}]\mathbf{R}_{\theta e} + [\mathbf{J}_{e1}\mathbf{O}]) \\ &\doteq \mathbf{J}_{1\theta}^T\mathbf{M}_P\widehat{\mathbf{J}}_{e1}, \qquad (37)\end{aligned}$$

where we have ultimately included only the payload terms.

LEMMA 3. As $\delta\mathbf{M}_{zz} \to \mathbf{O}$, the conditions of Lemma 1 are satisfied.

**Proof.** Using (36) and (37) gives $\mathbf{M}_{zz,rr}\mathbf{J}_{1\theta}^{-1}\widehat{\mathbf{J}}_{e1} = \mathbf{J}_{1\theta}^T\mathbf{M}_P\widehat{\mathbf{J}}_{1e} = \mathbf{M}_{zz,re}$. □

Let $\mathbf{M}_{\theta\theta}^{(i)}$ and $\mathbf{M}_{\theta e}^{(i)}$, $i = 1, 2$, denote the contributions from each arm to $\mathbf{M}_{\theta\theta}$ and $\mathbf{M}_{\theta e}$, respectively. The following Lemma shows that if the condition in (33) is satisfied by each arm, modeled as a single chain, then the corresponding closed-loop condition in Lemma 2 also holds.

LEMMA 4. If $\mathbf{M}_{\theta\theta}^{(i)}\mathbf{J}_{\theta i}^{-1}\mathbf{J}_{ei} = \mathbf{M}_{\theta e}^{(i)}$, $i = 1, 2$, then $\mathbf{M}_{zz,rr}^{(i)}\mathbf{J}_{\theta 1}^{-1}\widehat{\mathbf{J}}_{e1} = \mathbf{M}_{zz,re}^{(i)}$ where $\mathbf{M}_{zz,rr}^{(i)}$ and $\mathbf{M}_{zz,re}^{(i)}$ are the contributions to $\mathbf{M}_{zz,rr}$ and $\mathbf{M}_{zz,re}$, respectively, due to $\mathbf{M}_{\theta\theta}^{(i)}$ and $\mathbf{M}_{\theta e}^{(i)}$, $i = 1, 2$.

**Proof.** First consider $i = 1$. Then,

$$\begin{aligned}\mathbf{M}_{zz,rr}^{(1)} &= \mathbf{R}_{\theta r}^T\mathbf{M}_{\theta\theta}\mathbf{R}_{\theta r} = [\mathbf{1} \;\; \widehat{\mathbf{R}}_{\theta r}^T]\begin{bmatrix}\mathbf{M}_{\theta\theta}^{(1)} & \mathbf{O}\\ \mathbf{O} & \mathbf{O}\end{bmatrix}\begin{bmatrix}\mathbf{1}\\ \widehat{\mathbf{R}}_{\theta r}\end{bmatrix} \\ &= \mathbf{M}_{\theta\theta}^{(1)}\end{aligned}$$

and

$$\begin{aligned}\mathbf{M}_{zz,re}^{(1)} &= \mathbf{R}_{\theta r}^T[\mathbf{M}_{\theta\theta}\mathbf{R}_{\theta e} + \mathbf{M}_{\theta e}] \\ &= [\mathbf{1} \;\; \widehat{\mathbf{R}}_{\theta r}^T]\left\{\begin{bmatrix}\mathbf{M}_{\theta\theta}^{(1)} & \mathbf{O}\\ \mathbf{O} & \mathbf{O}\end{bmatrix}\begin{bmatrix}\mathbf{O}\\ \widehat{\mathbf{R}}_{\theta e}\end{bmatrix} + \begin{bmatrix}\mathbf{M}_{\theta e}^{(1)} & \mathbf{O}\\ \mathbf{O} & \mathbf{O}\end{bmatrix}\right\} \\ &= [\mathbf{M}_{\theta e}^{(1)} \;\; \mathbf{O}].\end{aligned}$$

Therefore, $\mathbf{M}_{zz,rr}^{(1)}\mathbf{J}_{1\theta}^{-1}\widehat{\mathbf{J}}_{1e} = \mathbf{M}_{\theta\theta}^{(1)}\mathbf{J}_{\theta 1}^{-1}[\mathbf{J}_{1e} \;\; \mathbf{O}] = [\mathbf{M}_{\theta e}^{(1)} \;\; \mathbf{O}] = \mathbf{M}_{zz,re}^{(1)}$.

When $i = 2$,

$$\begin{aligned}\mathbf{M}_{zz,rr}^{(2)} &= \mathbf{R}_{\theta r}^T\mathbf{M}_{\theta\theta}\mathbf{R}_{\theta r} = [\mathbf{1} \;\; \widehat{\mathbf{R}}_{\theta r}^T]\begin{bmatrix}\mathbf{O} & \mathbf{O}\\ \mathbf{O} & \mathbf{M}_{\theta\theta}^{(2)}\end{bmatrix}\begin{bmatrix}\mathbf{1}\\ \widehat{\mathbf{R}}_{\theta r}\end{bmatrix} \\ &= \widehat{\mathbf{R}}_{\theta r}^T\mathbf{M}_{\theta\theta}^{(2)}\widehat{\mathbf{R}}_{\theta r}\end{aligned}$$

and

$$\begin{aligned}\mathbf{M}_{zz,re}^{(2)} &= \mathbf{R}_{\theta r}^T[\mathbf{M}_{\theta\theta}\mathbf{R}_{\theta e} + \mathbf{M}_{\theta e}] \\ &= [\mathbf{1} \;\; \widehat{\mathbf{R}}_{\theta r}^T]\left\{\begin{bmatrix}\mathbf{O} & \mathbf{O}\\ \mathbf{O} & \mathbf{M}_{\theta\theta}^{(2)}\end{bmatrix}\begin{bmatrix}\mathbf{O}\\ \widehat{\mathbf{R}}_{\theta e}\end{bmatrix} + \begin{bmatrix}\mathbf{O} & \mathbf{O}\\ \mathbf{O} & \mathbf{M}_{\theta e}^{(2)}\end{bmatrix}\right\} \\ &= \widehat{\mathbf{R}}_{\theta r}^T\mathbf{M}_{\theta\theta}^{(2)}\widehat{\mathbf{R}}_{\theta e} + [\mathbf{O} \;\; \widehat{\mathbf{R}}_{\theta r}^T\mathbf{M}_{\theta e}^{(2)}]. \qquad (38)\end{aligned}$$

From (17), $\widehat{\mathbf{R}}_{\theta e,1} = \mathbf{J}_{\theta 2}^{-1}\mathbf{J}_{e1}$, $\widehat{\mathbf{R}}_{\theta e,2} = -\mathbf{J}_{\theta 2}^{-1}\mathbf{J}_{e2}$, and $\widehat{\mathbf{R}}_{\theta r} = -\mathbf{J}_{\theta 2}^{-1}\mathbf{J}_{\theta 1}$. Hence,

$$\begin{aligned}\mathbf{M}_{zz,rr}^{(2)}\mathbf{J}_{\theta 1}^{-1}\widehat{\mathbf{J}}_{e1} &= \widehat{\mathbf{R}}_{\theta r}^T\mathbf{M}_{\theta\theta}^{(2)}\widehat{\mathbf{R}}_{\theta r}\mathbf{J}_{\theta 1}^{-1}\widehat{\mathbf{J}}_{e1} \\ &= -\widehat{\mathbf{R}}_{\theta r}^T\mathbf{M}_{\theta\theta}^{(2)}\mathbf{J}_{\theta 2}^{-1}[\mathbf{J}_{e1} \;\; \mathbf{O}] \\ &= \widehat{\mathbf{R}}_{\theta r}^T\mathbf{M}_{\theta\theta}^{(2)}[\widehat{\mathbf{R}}_{\theta e,1} \;\; \mathbf{O}].\end{aligned}$$

Using (38) and the property stated in the lemma,

$$\begin{aligned}\mathbf{M}_{zz,re}^{(2)} &= \widehat{\mathbf{R}}_{\theta r}^T(\mathbf{M}_{\theta\theta}^{(2)}[\widehat{\mathbf{R}}_{\theta e,1} \;\; \widehat{\mathbf{R}}_{\theta e,2}] + [\mathbf{O} \;\; \mathbf{M}_{\theta\theta}^{(2)}\mathbf{J}_{\theta 2}^{-1}\mathbf{J}_{e2}]) \\ &= \widehat{\mathbf{R}}_{\theta r}^T\mathbf{M}_{\theta\theta}^{(2)}[\widehat{\mathbf{R}}_{\theta e,1} \;\; \mathbf{O}] \\ &= \mathbf{M}_{zz,rr}^{(2)}\mathbf{J}_{\theta 1}^{-1}\widehat{\mathbf{J}}_{e1},\end{aligned}$$

which establishes the result. □

The main utility of this result lies in the ability to apply the results of (Damaren 1998) to the closed-loop case. In particular, two planar 3-DoF arms manipulating a large payload will possess the nodal property leading to passivity in (32) even in the presence of large stator masses at the outboard end of each link. This is important because although the links can be made quite light, electromagnetic actuators will typically be large to meet the torque requirements of manipulating a large payload. This is an accurate depiction of the experimental apparatus used in Section 6.

## 5. Approximate Nonlinear Dynamics and Controller Design

Given a desired payload trajectory $\{\boldsymbol{\rho}_d, \dot{\boldsymbol{\rho}}_d, \ddot{\boldsymbol{\rho}}_d\}$, it is proposed to use a controller containing feedforward and feedback elements. The general paradigm for passivity-based control

is described by Ortega et al. (1998). The feedforward will typically be based on the motion equations and preserve the passivity property in the error dynamics. The goal here is to establish this using the asymptotic form of the dynamics corresponding to the property in Lemma 1. The kinetic energy can be written as $T = \frac{1}{2}\dot{\mathbf{q}}^T\mathbf{M}\dot{\mathbf{q}} = \frac{1}{2}\dot{\mathbf{z}}^T\mathbf{M}_{zz}\dot{\mathbf{z}}$ with $\mathbf{M}_{zz}$ as given in (20) with $\mathbf{z}^T = [\boldsymbol{\theta}_1^T \quad \mathbf{q}_e^T]$. Letting $\dot{\boldsymbol{\theta}}_1 = \mathbf{J}_{1\theta}^{-1}(\dot{\boldsymbol{\rho}} - \widehat{\mathbf{J}}_{1e}\dot{\mathbf{q}}_e)$ and using $\mathbf{M}_{zz,rr}\mathbf{J}_{\theta 1}^{-1}\widehat{\mathbf{J}}_{e1} = \mathbf{M}_{zz,re}$ leads to $T = T_\rho + T_e$, where

$$T_\rho = \frac{1}{2}\dot{\boldsymbol{\rho}}^T\mathbf{M}_{\rho\rho}\dot{\boldsymbol{\rho}}, \quad \mathbf{M}_{\rho\rho} \triangleq \mathbf{J}_{1\theta}^{-T}\mathbf{M}_{zz,rr}\mathbf{J}_{1\theta}^{-1}, \tag{39}$$

$$T_e = \frac{1}{2}\dot{\mathbf{q}}_e^T\widehat{\mathbf{M}}_{ee}\dot{\mathbf{q}}_e, \quad \widehat{\mathbf{M}}_{ee} \triangleq \mathbf{M}_{zz,ee} - \mathbf{M}_{zz,re}^T\mathbf{M}_{zz,rr}^{-1}\mathbf{M}_{zz,re}. \tag{40}$$

The potential energy is $V_e = \frac{1}{2}\mathbf{q}_e^T\mathbf{K}_{ee}\mathbf{q}_e$, and using the choice of torques in (28), the virtual work can be written as $\delta W_e = \boldsymbol{\tau}^T\delta\boldsymbol{\theta} = \widehat{\boldsymbol{\tau}}^T[C_1\mathbf{J}_{\theta 1}\delta\boldsymbol{\theta}_1 + C_2\mathbf{J}_{2\theta}\delta\boldsymbol{\theta}_2] = \widehat{\boldsymbol{\tau}}^T[\delta\boldsymbol{\rho} - C_1\mathbf{J}_{e1}\delta\mathbf{q}_{e1} - C_2\mathbf{J}_{e2}\delta\mathbf{q}_{e2}]$. Lagrange's equations with generalized coordinates $\{\boldsymbol{\rho}, \mathbf{q}_e\}$, in conjunction with the work and energy expressions, yield

$$\mathbf{M}_{\rho\rho}\ddot{\boldsymbol{\rho}} = \widehat{\boldsymbol{\tau}} + \mathbf{f}_{non,\rho} \tag{41}$$

$$\widehat{\mathbf{M}}_{ee}\ddot{\mathbf{q}}_e + \mathbf{K}_{ee}\mathbf{q}_e = -[C_1\mathbf{J}_{e1} \quad C_2\mathbf{J}_{e2}]^T\widehat{\boldsymbol{\tau}} + \mathbf{f}_{non,e}, \tag{42}$$

with

$$\mathbf{f}_{non,\rho} = -\dot{\mathbf{M}}_{\rho\rho}\dot{\boldsymbol{\rho}} + \frac{1}{2}\partial(\dot{\boldsymbol{\rho}}^T\mathbf{M}_{\rho\rho}\dot{\boldsymbol{\rho}} + \dot{\mathbf{q}}_e^T\widehat{\mathbf{M}}_{ee}\dot{\mathbf{q}}_e)/\partial\boldsymbol{\rho}, \tag{43}$$

$$\mathbf{f}_{non,e} = -\dot{\widehat{\mathbf{M}}}_{ee}\dot{\mathbf{q}}_e + \frac{1}{2}\partial(\dot{\boldsymbol{\rho}}^T\mathbf{M}_{\rho\rho}\dot{\boldsymbol{\rho}} + \dot{\mathbf{q}}_e^T\widehat{\mathbf{M}}_{ee}\dot{\mathbf{q}}_e)/\partial\mathbf{q}_e. \tag{44}$$

These are coupled by virtue of the configuration dependence of $\mathbf{M}_{\rho\rho}$, $\widehat{\mathbf{M}}_{ee}$, $\mathbf{J}_\theta$, and $\mathbf{J}_e$.

The mass matrices $\mathbf{M}_{\rho\rho}$ and $\widehat{\mathbf{M}}_{ee}$ depend on $\boldsymbol{\theta}$ and $\mathbf{q}_e$, but a suitable approximation is to neglect the elastic coordinate dependence and take $\mathbf{M}_{\rho\rho}(\boldsymbol{\rho})$, $\widehat{\mathbf{M}}_{ee}(\boldsymbol{\rho})$ with $\boldsymbol{\theta}_i = \mathcal{F}_{ri}^{-1}(\boldsymbol{\rho})$, where $\mathcal{F}_{ri}^{-1}(\cdot), i = 1, 2$, are the rigid inverse kinematics maps. If one further neglects the $\mathcal{O}(\|\dot{\mathbf{q}}_e\|^2)$ term in (43), it becomes equivalent to the rigid-body *task-space* motion equations:

$$\mathbf{M}_{\rho\rho}\ddot{\boldsymbol{\rho}} + \mathbf{C}_\rho(\boldsymbol{\rho}, \dot{\boldsymbol{\rho}})\dot{\boldsymbol{\rho}} = \widehat{\boldsymbol{\tau}},$$

$$\mathbf{C}_\rho(\boldsymbol{\rho}, \dot{\boldsymbol{\rho}})\dot{\boldsymbol{\rho}} = \dot{\mathbf{M}}_{\rho\rho}\dot{\boldsymbol{\rho}} - \frac{1}{2}\partial(\dot{\boldsymbol{\rho}}^T\mathbf{M}_{\rho\rho}\dot{\boldsymbol{\rho}})/\partial\boldsymbol{\rho}, \tag{45}$$

where $\mathbf{C}_\rho(\boldsymbol{\rho}, \dot{\boldsymbol{\rho}})$ can be constructed so that $\dot{\mathbf{M}} - 2\mathbf{C}_\rho$ is skew-symmetric. A further simplification is possible if one includes only the payload contributions to $\mathbf{M}_{\rho\rho}$. Using the definition in (39) and the approximation in (36) gives $\mathbf{M}_{\rho\rho} = \mathbf{M}_P$. In general, $\mathbf{M}_P$ will be configuration dependent since it is the body mass matrix expressed relative to the absolute Cartesian frame. However, for planar geometries with $\boldsymbol{\rho}$ locating the payload mass center, $\mathbf{M}_P$ is constant and hence $\mathbf{C}_\rho = \mathbf{O}$.

Given the neglect of $\mathbf{q}_e$ in the mass matrices, the elastic motion equation can be simplified. The last two terms in (44) are neglected leaving $\mathbf{f}_{non,e} = -\dot{\widehat{\mathbf{M}}}_{ee}\dot{\mathbf{q}}_e$. Since the elastic equations have been generated under the assumption that the payload is nodal, the elastic energy for unforced motion is $T_e + V_e$ and its derivative is

$$\dot{T}_e + \dot{V}_e = \dot{\mathbf{q}}_e^T(\widehat{\mathbf{M}}_{ee}\ddot{\mathbf{q}}_e + \mathbf{K}_{ee}\mathbf{q}_e + \frac{1}{2}\dot{\widehat{\mathbf{M}}}_{ee}\dot{\mathbf{q}}_e)$$

$$= -\frac{1}{2}\dot{\mathbf{q}}_e^T\dot{\widehat{\mathbf{M}}}_{ee}\dot{\mathbf{q}}_e.$$

Arguing that $T_e + V_e$ should be conserved, $\dot{\widehat{\mathbf{M}}}_{ee}$ is skew-symmetric but since $\widehat{\mathbf{M}}_{ee}$ is symmetric, it should be taken as constant. This suggests that the vibration frequencies and the elastic components $\{\mathbf{q}_{1e,\alpha}, \mathbf{q}_{2e,\alpha}\}$ of the modes should be independent of configuration, a fact that has been observed numerically in the large payload case. However, the joint participation in each mode will be governed by $\boldsymbol{\theta}_{i,\alpha} = -\mathbf{J}_{i\theta}^{-1}(\boldsymbol{\theta})\mathbf{J}_{i,e}(\boldsymbol{\theta})\mathbf{q}_{ie,\alpha}$, which depends on configuration via the Jacobians. Hence, we adopt

$$\widehat{\mathbf{M}}_{ee}\ddot{\mathbf{q}}_e + \mathbf{K}_{ee}\mathbf{q}_e = -[C_1\mathbf{J}_{1e} \quad C_2\mathbf{J}_{2e}]^T\widehat{\boldsymbol{\tau}} \tag{46}$$

as the elastic motion equation.

### *5.1. Controller Design*

Given the desired trajectory $\boldsymbol{\rho}_d$, let $\widehat{\boldsymbol{\tau}}_d$ denote the feedforward signal, which will be defined momentarily. The corresponding desired behavior for the elastic displacements is defined by

$$\widehat{\mathbf{M}}_{ee}\ddot{\mathbf{q}}_{ed} + \mathbf{K}_{ee}\mathbf{q}_{ed} = -[C_1\mathbf{J}_{e1} \quad C_2\mathbf{J}_{e2}]^T\widehat{\boldsymbol{\tau}}_d, \tag{47}$$

and the desired form of $\boldsymbol{\rho}_\mu$ is defined by $\dot{\boldsymbol{\rho}}_{\mu d} = \dot{\boldsymbol{\rho}}_d - (1 - \mu)[C_1\mathbf{J}_{e1}\dot{\mathbf{q}}_{1ed} + C_2\mathbf{J}_{2e}\dot{\mathbf{q}}_{2ed}]$. Tracking errors are defined as $\widetilde{\boldsymbol{\rho}} = \boldsymbol{\rho} - \boldsymbol{\rho}_d$, $\widetilde{\boldsymbol{\rho}}_\mu = \boldsymbol{\rho}_\mu - \boldsymbol{\rho}_{\mu d}$, $\widetilde{\mathbf{q}}_e = \mathbf{q}_e - \mathbf{q}_{ed}$, and the filtered error is $\mathbf{s}_\mu = \dot{\widetilde{\boldsymbol{\rho}}}_\mu + \boldsymbol{\Lambda}\widetilde{\boldsymbol{\rho}}_\mu$ with $\boldsymbol{\Lambda} = \boldsymbol{\Lambda}^T > \mathbf{O}$. The virtual reference trajectory is defined by $\dot{\boldsymbol{\rho}}_r = \dot{\boldsymbol{\rho}}_d - \boldsymbol{\Lambda}\widetilde{\boldsymbol{\rho}}_\mu$ and the corresponding error by $\dot{\widetilde{\boldsymbol{\rho}}}_r = \dot{\boldsymbol{\rho}} - \dot{\boldsymbol{\rho}}_r = \dot{\widetilde{\boldsymbol{\rho}}} + \boldsymbol{\Lambda}\widetilde{\boldsymbol{\rho}}_\mu$.

The chosen feedforward is

$$\mathbf{M}_{\rho\rho}(\boldsymbol{\rho})\ddot{\boldsymbol{\rho}}_r + \mathbf{C}_\rho(\boldsymbol{\rho}, \dot{\boldsymbol{\rho}})\dot{\boldsymbol{\rho}}_r = \widehat{\boldsymbol{\tau}}_d. \tag{48}$$

Subtracting this from (45) and (47) from (46) gives

$$\mathbf{M}_{\rho\rho}(\boldsymbol{\rho})\ddot{\widetilde{\boldsymbol{\rho}}}_r + \mathbf{C}_\rho(\boldsymbol{\rho}, \dot{\boldsymbol{\rho}})\dot{\widetilde{\boldsymbol{\rho}}}_r = \widehat{\boldsymbol{\tau}} - \widehat{\boldsymbol{\tau}}_d \tag{49}$$

$$\widehat{\mathbf{M}}_{ee}\ddot{\widetilde{\mathbf{q}}}_e + \mathbf{K}_{ee}\widetilde{\mathbf{q}}_e = -[C_1\mathbf{J}_{e1} \quad C_2\mathbf{J}_{e2}]^T(\widehat{\boldsymbol{\tau}} - \widehat{\boldsymbol{\tau}}_d). \tag{50}$$

Now consider the function

$$\mathcal{V} = \frac{1}{2}\dot{\widetilde{\boldsymbol{\rho}}}_r^T\mathbf{M}_{\rho\rho}\dot{\widetilde{\boldsymbol{\rho}}}_r + \frac{1}{2}(1 - \mu)[\dot{\widetilde{\mathbf{q}}}_e^T\widehat{\mathbf{M}}_{ee}\dot{\widetilde{\mathbf{q}}}_e + \widetilde{\mathbf{q}}_e^T\widehat{\mathbf{K}}_{ee}\widetilde{\mathbf{q}}_e]. \tag{51}$$

Its time derivative is

$$\begin{aligned}\dot{\mathcal{V}} &= \dot{\tilde{\boldsymbol{\rho}}}_r^T(\frac{1}{2}\dot{\mathbf{M}}_{\rho\rho}\dot{\tilde{\boldsymbol{\rho}}}_r + \mathbf{M}_{\rho\rho}\ddot{\tilde{\boldsymbol{\rho}}}_r) \\ &\quad + (1-\mu)[\dot{\tilde{\mathbf{q}}}_e^T(\widehat{\mathbf{M}}_{ee}\ddot{\tilde{\mathbf{q}}}_e + \widehat{\mathbf{K}}_{ee}\tilde{\mathbf{q}}_e)] \\ &= \dot{\tilde{\boldsymbol{\rho}}}_r^T(\widehat{\boldsymbol{\tau}} - \widehat{\boldsymbol{\tau}}_d) - (1-\mu)\dot{\tilde{\mathbf{q}}}_e^T[C_1\mathbf{J}_{e1}\ \ C_2\mathbf{J}_{e2}]^T(\widehat{\boldsymbol{\tau}} - \widehat{\boldsymbol{\tau}}_d) \\ &= \mathbf{s}_\mu^T(\widehat{\boldsymbol{\tau}} - \widehat{\boldsymbol{\tau}}_d). \end{aligned} \quad (52)$$

Integration of this establishes passivity from $(\widehat{\boldsymbol{\tau}} - \widehat{\boldsymbol{\tau}}_d)$ to $\mathbf{s}_u$ and selecting a strictly passive feedback, say

$$\widehat{\boldsymbol{\tau}} = \widehat{\boldsymbol{\tau}}_d - \mathbf{K}_d\mathbf{s}_\mu, \quad \mathbf{K}_d = \mathbf{K}_d^T > \mathbf{O}, \quad (53)$$

yields $\dot{\mathcal{V}} = -\mathbf{s}_\mu^T\mathbf{K}_d\mathbf{s}_\mu$. Hence, $\mathbf{s}_\mu \in L_2$, and it follows from a standard result (Ortega et al., 1998, Lemma A.12) that $\tilde{\boldsymbol{\rho}}_\mu \in L_2$ and $\tilde{\boldsymbol{\rho}}_\mu \to \mathbf{0}$ as $t \to \infty$. It is also possible to show that $\tilde{\boldsymbol{\rho}} \to \mathbf{0}$ under additional hypotheses that guarantee that $\tilde{\mathbf{q}}_e \to \mathbf{0}$ (Damaren 1996b). The final form of the control law follows from combining (28), (48), and (53):

$$\begin{aligned}\boldsymbol{\tau} = [C_1\mathbf{J}_{1\theta}(\boldsymbol{\theta}_1) \quad C_2\mathbf{J}_{2\theta}(\boldsymbol{\theta}_2)]^T[\mathbf{M}_{\boldsymbol{\rho\rho}}(\ddot{\boldsymbol{\rho}}_d - \boldsymbol{\Lambda}\dot{\tilde{\boldsymbol{\rho}}}_\mu) \\ + \mathbf{C}_\rho(\boldsymbol{\rho},\dot{\boldsymbol{\rho}})(\dot{\boldsymbol{\rho}}_d - \boldsymbol{\Lambda}\tilde{\boldsymbol{\rho}}_\mu) - \mathbf{K}_d(\dot{\tilde{\boldsymbol{\rho}}}_\mu + \boldsymbol{\Lambda}\tilde{\boldsymbol{\rho}}_\mu)]. \end{aligned} \quad (54)$$

In the implementation that follows, the approximation $\boldsymbol{\rho}_{\mu d} \doteq \boldsymbol{\rho}_d$ is made so that $\tilde{\boldsymbol{\rho}}_\mu = \boldsymbol{\rho}_\mu - \boldsymbol{\rho}_d$ with $\boldsymbol{\rho}_\mu$ calculated using (9).

## 6. Experimental Results

In this section, the controller will be implemented on a testbed consisting of two flexible arms manipulating a rigid body. A photograph is shown in Figure 2 and a schematic representation is shown in Figure 3. The two bodies in each arm ($\mathcal{B}_1$, $\mathcal{B}_2$ and $\mathcal{B}_4$, $\mathcal{B}_5$) are modeled as an inboard rigid assembly (rotor), a homogeneous isotropic flexible link, and an outboard rigid body (stator). The links are 6 mm thick aluminum. The payload central body consists of an aluminum cannister containing steel rigid rings with inertia augmentation via cantilevered lead blocks. It is connected to the wrist motors of each arm via two steel links. The entire assembly is modeled as a single rigid payload body, $\mathcal{B}_3$. The mass properties of each body are presented in Table 2. The first ($c$) and second ($J$) mass moments are taken relative to the corresponding inboard attachment point for that segment.

The six motors are standard brushed DC motors driving through low backlash planetary gearheads. The motor rotor inertias are effectively multiplied by the square of the gear ratio and are lumped with the joint degree of freedom. This is distinct from the inboard rotor asseblies, which are associated with the total (absolute) angular velocity of the joint. The motor rotor inertias are given in Table 2.

The in-plane bending of each link is modeled using Euler-Bernoulli beam theory with spatial discretization according to

$$v_n(x,t) = \sum_{i=1}^{n_e} q_{en,i}(t)\psi_i(x),$$

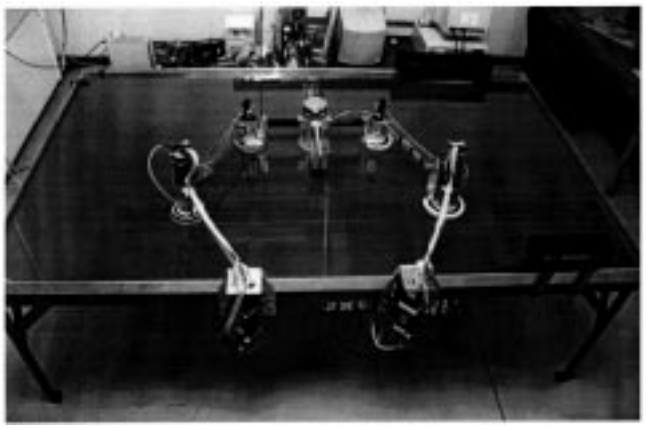

Fig. 2. Experimental robot (photograph).

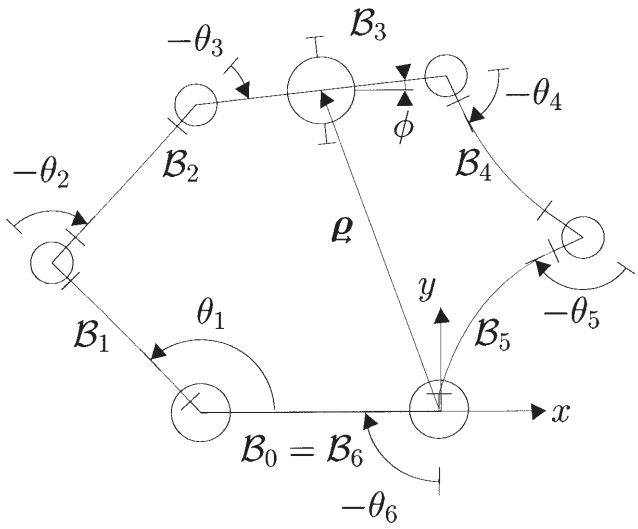


Fig. 3. Experimental robot (schematic).

where $x$ is the coordinate along the neutral axis with $x = 0$ coinciding with the attachment to the rotor. Although the polynomials $\psi_i(x) = x^{i+1}$ have worked extremely well for open-chain versions of the system under study, they had poor convergence characteristics for the closed-loop problem. Better performance was obtained by choosing the $\psi_i(x)$ to be the exact cantilevered free bending modes of a uniform beam. For the simulation results to follow, two such modes were used for each link. The results of eigenproblem in eq. (22) were obtained using 10 modes per link.

Encoders at each joint are used to measure the angles, and simple differencing was used to obtain their rates. Three strain gages on each of links 4 and 5 are used to fit the coefficients in an assumed deflection profile of the form $v_n(x,t) = q_{en,1}(t)x^2 + q_{en,2}(t)x^3$. The payload position $\boldsymbol{\rho}(\boldsymbol{\theta}_2, \mathbf{q}_{2e})$ was then calculated by forward kinematics and the prediction was validated using a 2D CCD camera placed above the table. Simple differencing was again used to determine $\dot{\boldsymbol{\rho}}$. It was found that the CCD measurement failed to

**Table 1. Robot Mass Properties**

| | $\ell$ (m) | $m$ (kg) | $c$ (g·m) | $J$ (g·m$^2$) | $EI$ (N·m$^2$) |
|---|---|---|---|---|---|
| Base ($\mathcal{B}_0$) | 0.600 | | | | |
| Arm 1 | | | | | |
| $\mathcal{B}_1$ rotor | 0.037 | 2.657 | 1.84 | 0.232 | |
| $\mathcal{B}_1$ link | 0.406 | 0.196 | 40.4 | 10.9 | 39.3 |
| $\mathcal{B}_1$ stator | 0.062 | 1.924 | 112. | 8.43 | |
| $\mathcal{B}_2$ rotor | 0.082 | 1.802 | 15.8 | 2.19 | |
| $\mathcal{B}_2$ link | 0.360 | 0.177 | 32.3 | 7.76 | 39.3 |
| $\mathcal{B}_2$ stator | 0.067 | 0.934 | 54.6 | 4.15 | |
| Payload ($\mathcal{B}_3$) | 0.598 | 15.71 | 4667 | 1951 | |
| Arm 2 | | | | | |
| $\mathcal{B}_4$ rotor | 0.067 | 0.934 | 7.99 | 1.02 | |
| $\mathcal{B}_4$ link | 0.327 | 0.188 | 26.1 | 9.69 | 39.3 |
| $\mathcal{B}_4$ stator | 0.112 | 2.100 | 206. | 24.3 | |
| $\mathcal{B}_5$ rotor | 0.077 | 2.234 | 10.2 | 3.26 | |
| $\mathcal{B}_5$ link | 0.390 | 0.157 | 37.3 | 5.69 | 39.3 |
| $\mathcal{B}_5$ stator | 0.037 | 2.532 | 92.5 | 131.3 | |

**Table 2. Rotor Inertias**

| joint | (g·m$^2$) | (g·m$^2$) |
|---|---|---|
| 1, 6 | 127.8 | 127.8 |
| 2, 5 | 150.4 | 306.9 |
| 3, 4 | 16.05 | 16.05 |

**Table 3. Experimental Frequencies**

| $\alpha$ | $\omega_\alpha$ (Hz) numerical | $\omega_\alpha$ (Hz) expt. |
|---|---|---|
| 1 | 4.1 | 4.1 |
| 2 | 5.4 | 4.6 |
| 3 | 8.4 | 7.6 |
| 4 | 9.8 | 7.6 |
| 5 | 27.3 | 15.3 |
| 6 | 29.6 | 15.2 |

provide a good rate measurement under differencing on account of quantization effects. Torque control of each motor is accomplished using a high-gain PI law for current driving the motor voltage through a standard H-bridge.

Prior to examining the experimental tracking, the mode shapes corresponding to (22) for the configuration $\boldsymbol{\rho} = [-0.3\,\text{m}\ 0.8\,\text{m}\ 0]^T$ are given in Figure 4. The numerical frequencies and the experimental ones, obtained by sinusoidal torque sweeps, are shown in Table 3. The agreement is good for the two lowest modes but grows progressively worse. For each vibration mode, the quality of the node at the endpoint has been evaluated according to

$$\mathsf{J}_\alpha = \frac{||\boldsymbol{\rho}_\alpha||_2}{\frac{1}{2}||\mathbf{J}_{1\theta}\boldsymbol{\theta}_{1\alpha} + \mathbf{J}_{2\theta}\boldsymbol{\theta}_{2\alpha}||_2}, \tag{55}$$

where $||(\cdot)||_2$ denotes the Euclidean norm in three-space. For $\alpha = 2, 5$, and 6, $\mathsf{J}_\alpha < 0.06$, which corresponds to modes that are largely confined to Arm 1. For $\alpha = 1, 3$, and 4, $\mathsf{J}_\alpha$ is not as small. The difference between the two sets of modes can be attributed to the larger motor rotor inertia at the elbow of arm 2. As noted in Damaren (1998), the rotor inertia is the dominant agent in lessening the quality of the payload node.

To gage the effect of the payload size on $\mathsf{J}_\alpha$, $\mathbf{M}_P$ was replaced with $\epsilon_P \mathbf{M}_P$ and $\mathsf{J}_\alpha$ determined as a function of $\epsilon_P$ for the first six vibration modes (see Fig. 5). The configuration dependence on $\mathsf{J}_\alpha$ is shown in Figure 6 where $\mathsf{J}_\alpha$ is plotted as a function of payload position as $y$ is varied from 0.9 to 0.3 m for fixed $x = -0.3$ m and $\phi = 0$. The corresponding frequency variation is shown in Figure 7 and supports the assumption regarding the constancy of $\widehat{\mathbf{M}}_{ee}$.

The first maneuver is a straight line connecting $\boldsymbol{\rho}_0 = [-0.6\,\text{m}\ 0.8\,\text{m}\ 0]^T$ to $\boldsymbol{\rho}_T = [0\ 0.8\,\text{m}\ 0]^T$ in $T = 2$ sec. The desired trajectory for $\boldsymbol{\rho}(t)$ is obtained by applying forward kinematics to joint trajectories obeying quintic polynomials matching $\dot{\theta}_n(0) = \ddot{\theta}_n(0) = \dot{\theta}_n(T) = \ddot{\theta}_n(T) = 0$ and the required endpoints. The controller is selected according to (54) with, $\mathbf{M}_{\rho\rho} \doteq \mathbf{M}_P = \text{diag}\{m_P, m_P, J_P\}$, with $m_P = 15.7$ kg, $J_P = 0.537\ \text{kg}\cdot\text{m}^2$, and $\mathbf{C}_\rho = \mathbf{O}$. The gains are chosen such that

$$\mathbf{K}_d\boldsymbol{\Lambda} = \Omega_c^2\mathbf{M}_P, \quad \mathbf{K}_d + \mathbf{M}_P\boldsymbol{\Lambda} = 2\zeta\Omega_c\mathbf{M}_P, \tag{56}$$

with $\Omega_c = 2.3$ rad/s and $\zeta_c = 0.4$. The value of $\mu$ is 0.8.

The desired, simulated, and experimental task space trajectories are shown in Figure 8 for $C_1 = C_2 = 0.5$. Also

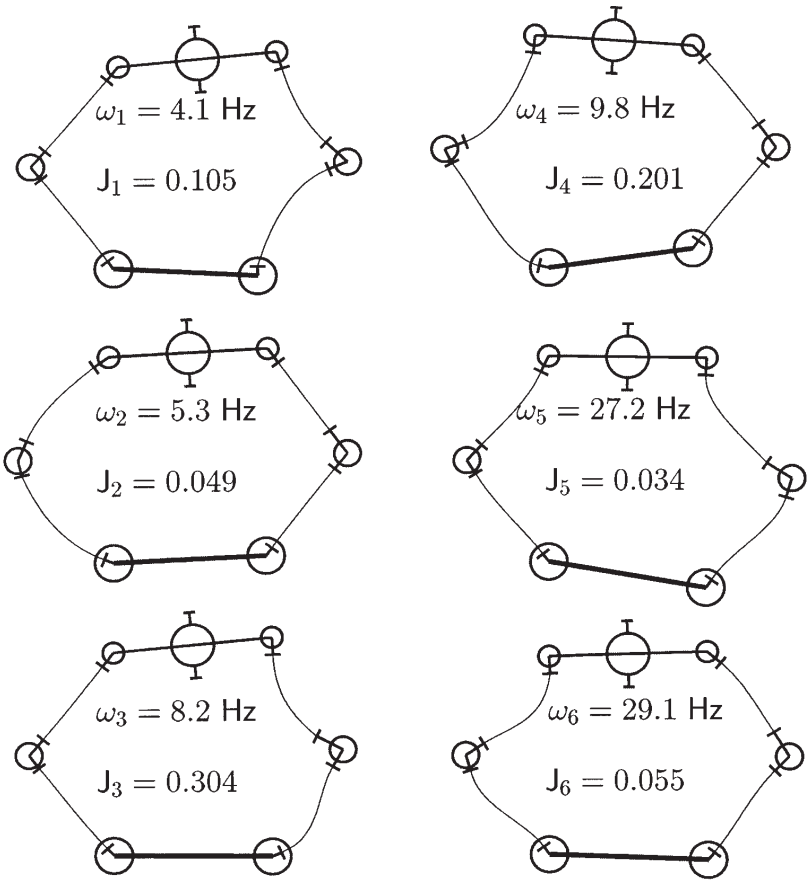


Fig. 4. Unconstrained mode shapes ($\rho = [-0.3m\, 0.8m\, 0]^T$).

shown are the tip deflections at the "end" of links 4 and 5 (i.e., at joints 4 and 5, respectively). Here, the desired curves correspond to the static solution of (47), i.e., $\widehat{\mathbf{M}}_{ee} = \mathbf{O}$, with $\widehat{\boldsymbol{\tau}}_d = \widehat{\boldsymbol{\tau}}$. The tracking is reasonably good and agrees well with the simulation prediction. The joint angle trajectories are shown in Figure 9. As expected, the simulation and experimental results do not follow the rigid trajectory very well but show reasonable agreement with each other, especially joints 1 and 3. Task space and link deflections are shown in Figures 10 and 11 for $C_1 = 0.25$ and $C_1 = 0.75$, respectively. The payload tracking is as good as $C_1 = 0.5$ and demonstrates the success of the load-sharing scheme.

The second trajectory is a circle with constant orientation ($\phi = 0$) for the payload. The center of the circle is given by $x_c = -0.3$, $y_c = 0.75$, and its radius is $r_c = 0.15$ m. The angle $\psi(t)$ measures the payload position around the circle with $\psi(t) = 0$ corresponding to the "3 o'clock" position. It is selected so that the first semicircle is an acceleration phase with $\psi(0) = \pi/2$, $\dot{\psi}(0) = 0$, $\ddot{\psi}(0) = 0$, $\dot{\psi}(T) = 2\pi/T$, and $\ddot{\psi}(T) = 0$ with

$$\psi(t) = \frac{\pi}{2} + \frac{\pi t}{T} - \sin\frac{\pi t}{T}.$$

The next three circles are performed with $\dot{\psi} = 2\pi/T$ (constant), and the last semicircle is a deceleration phase terminating with $\psi(5T) = \pi/2$ and $\dot{\psi}(5T) = \ddot{\psi}(5T) = 0$, with $\psi(5T - t) = \pi - \psi(t)$, $0 \le t \le T$. The payload tracking and link deflections are shown in Figure 12 for $C_1 = C_2 = 0.5$ using the same controller parameters as before except $\mu = 0.92$. The predictions for the link deflections agree quite well, but the experimental $y$-tracking is not very good. For this maneuver, the elbow angles experience large angular accelerations and the absence of their rotor contributions to the feedforward plays a large part in the discrepancy.

## 7. Conclusions

A passivity-based controller has been developed for the manipulation of large rigid payloads by two lightweight flexible robot arms. Payload nodal properties for the vibration modes, which are present for each arm viewed as an open chain, were shown to be inherited by the closed-loop system. This property was used to show that the $\mu$-tip rate was passive with respect to a suitably defined torque input. The nonlinear equations of motion consistent with the linearized modal ideas

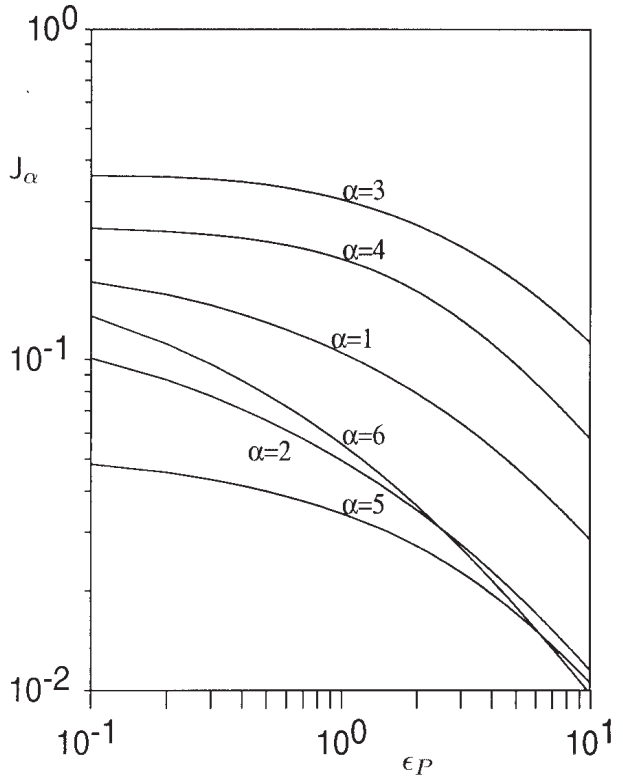


Fig. 5. Payload nodal quality versus payload size ($\rho = [-0.3m 0.8m 0]^T$).

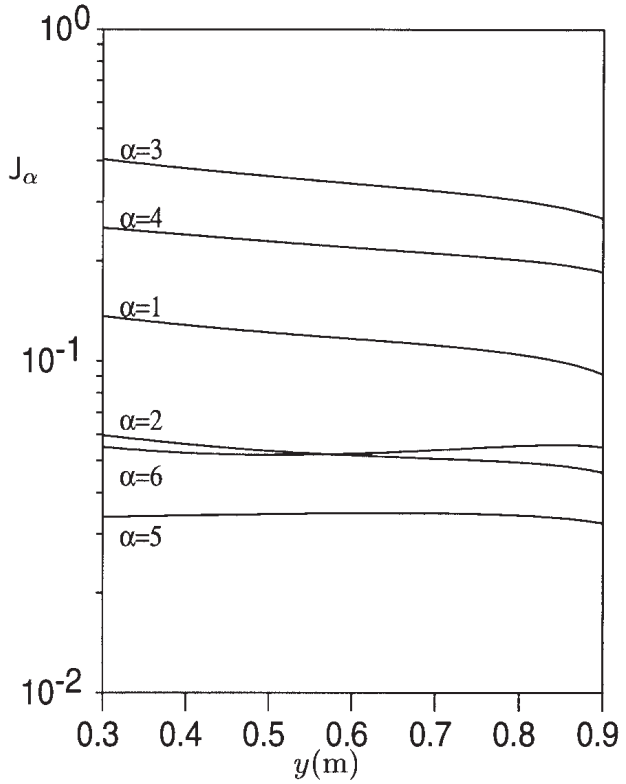


Fig. 6. Payload nodal quality versus $y$-configuration ($x = -0.3m, \phi = 0$).

were developed by formulating the nodal condition in terms of the the system's kinematical and dynamical matrices. A free load-sharing parameter was introduced and its symmetric use in forming the passive output as well as distributing the torques was key to the passivity arguments.

The experimental implementation of the controllers showed reasonably good tracking and vibration suppression. Furthermore, a simulation methodology was validated experimentally, which extended key techniques from the forward dynamics problem of rigid closed-loop systems.

The results presented here, when viewed with their counterparts for open flexible chains, demonstrate that the $\mu$-tip rate is an effective and relatively simple way of coping with difficulties incurred by noncollocation in flexble systems manipulating large objects.

## Acknowledgments

The author gratefully acknowledges financial support provided by the University of Canterbury in the form of Research Grants 2201999 and 2314034. The work presented here would not have been possible without the assistance of Andrew Cree and Eftychios Christoforou.

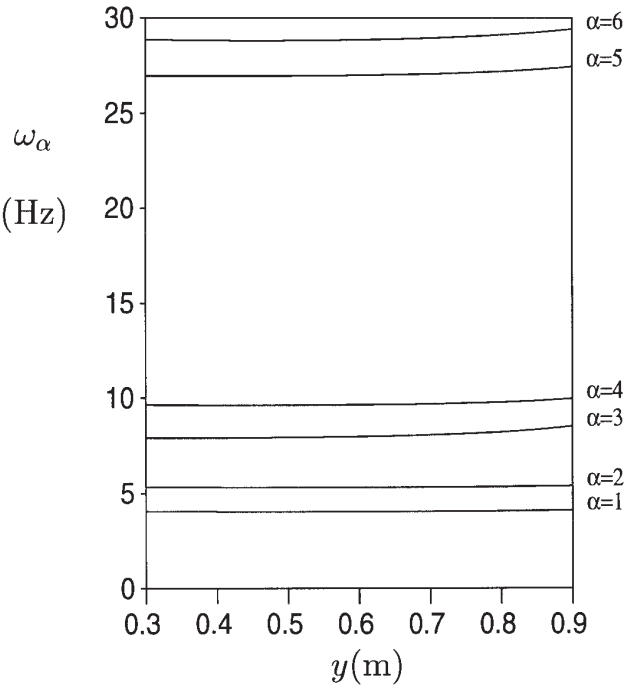


Fig. 7. Vibration frequencies versus $y$-configuration ($x = -0.3m, \phi = 0$).

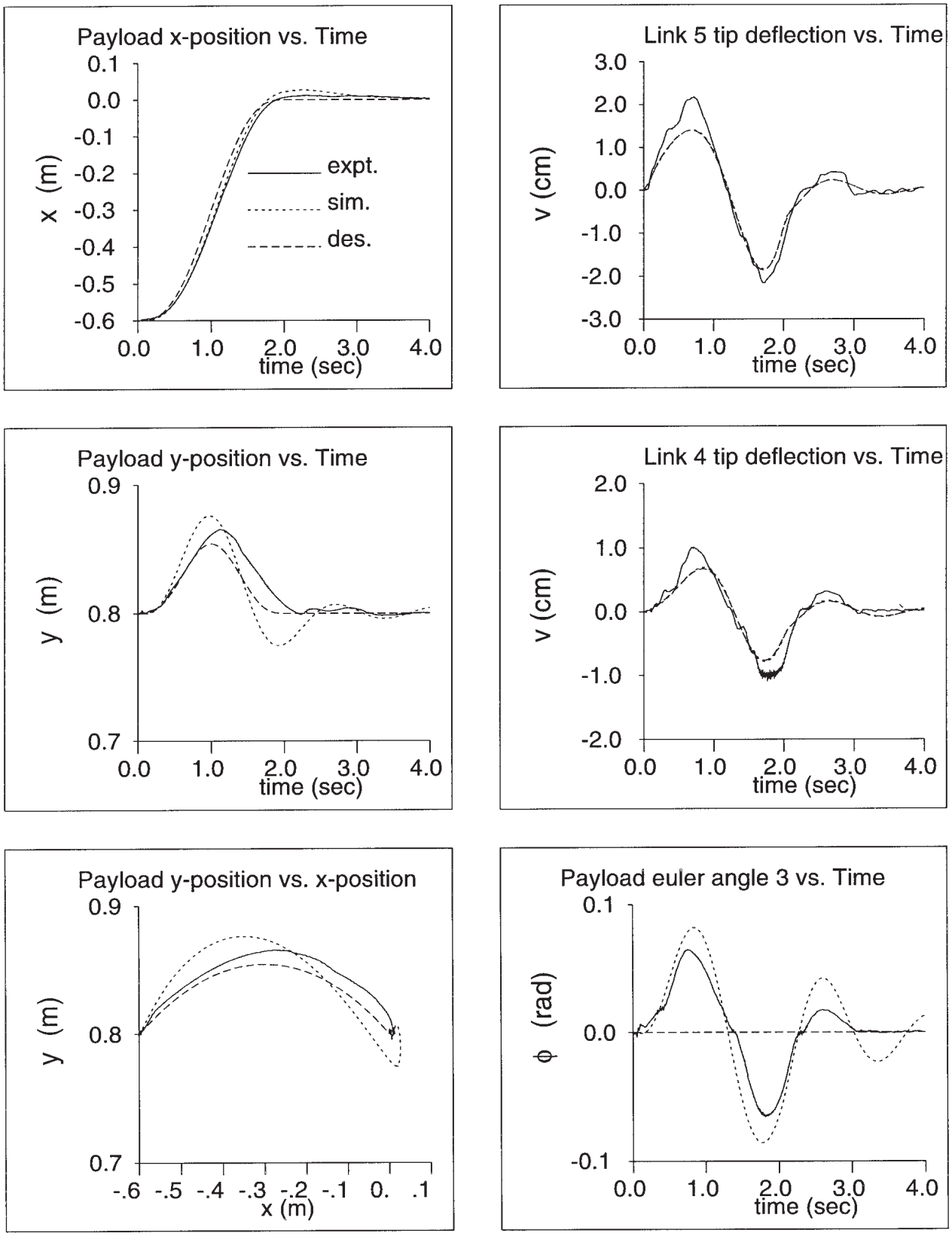


Fig. 8. Results for $x$-translation ($C_1 = 0.5$, $C_2 = 0.5$).

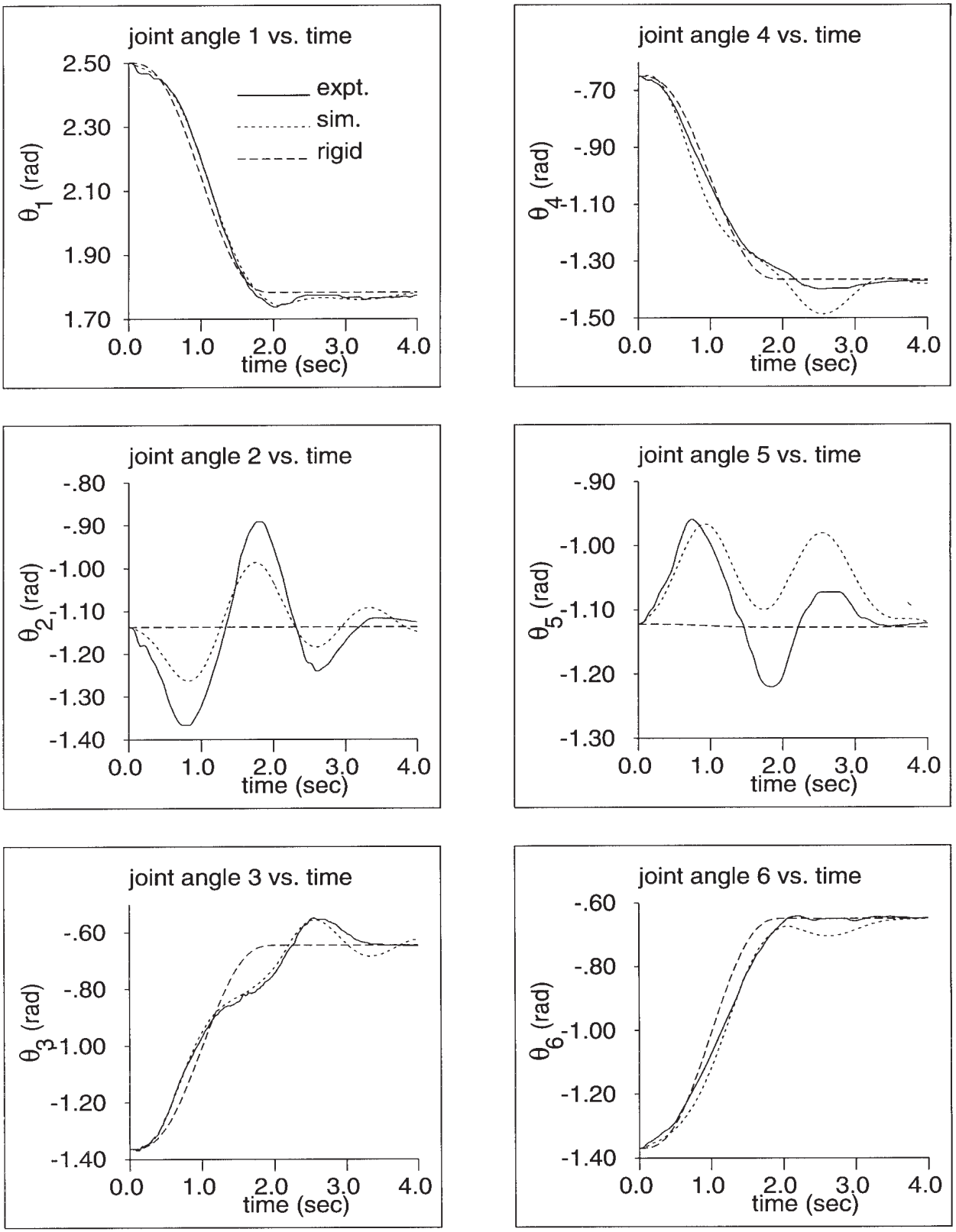


Fig. 9. Joint angles for $x$-translation ($C_1 = 0.5$, $C_2 = 0.5$).

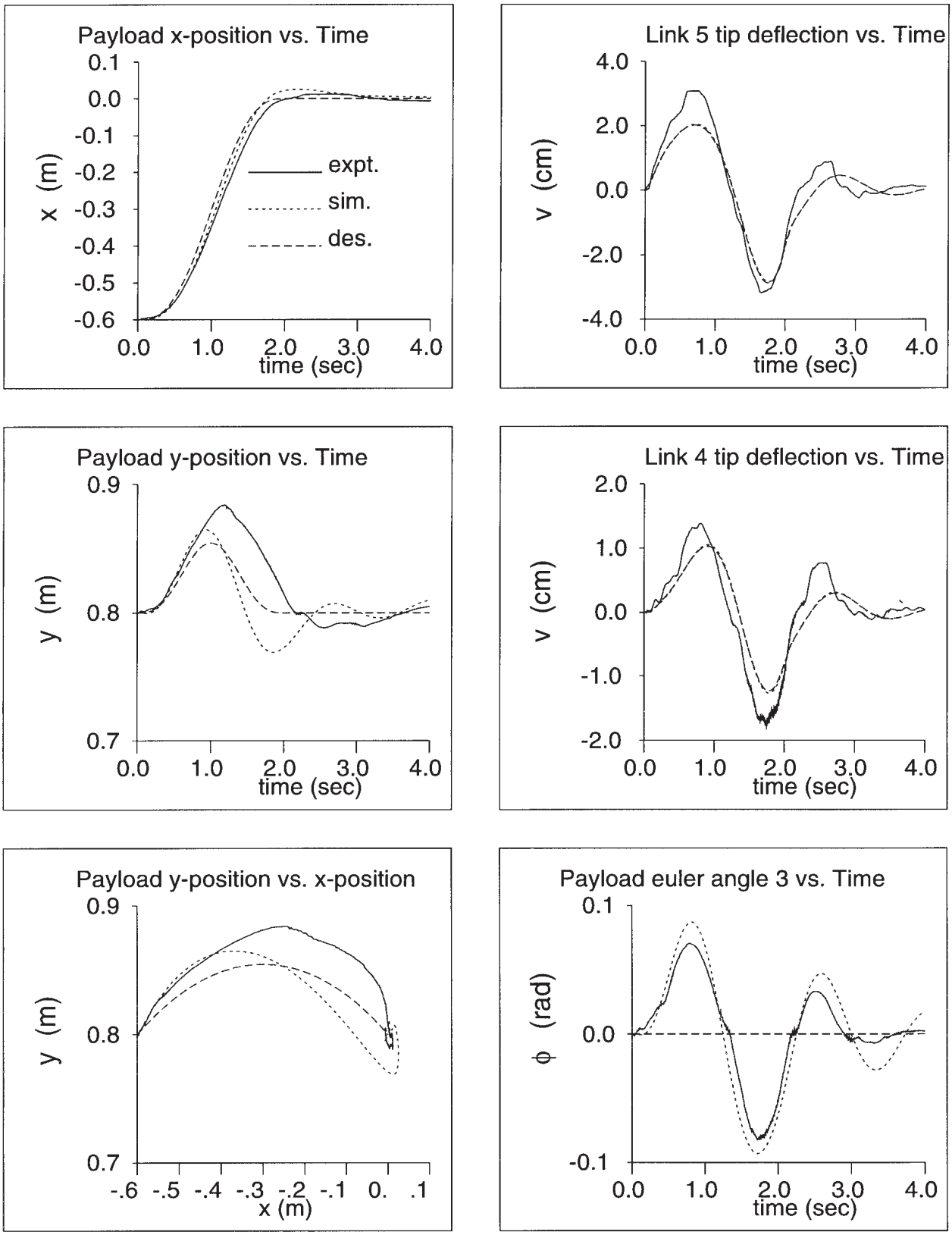


Fig. 10. Results for $x$-translation ($C_1 = 0.25$, $C_2 = 0.75$).

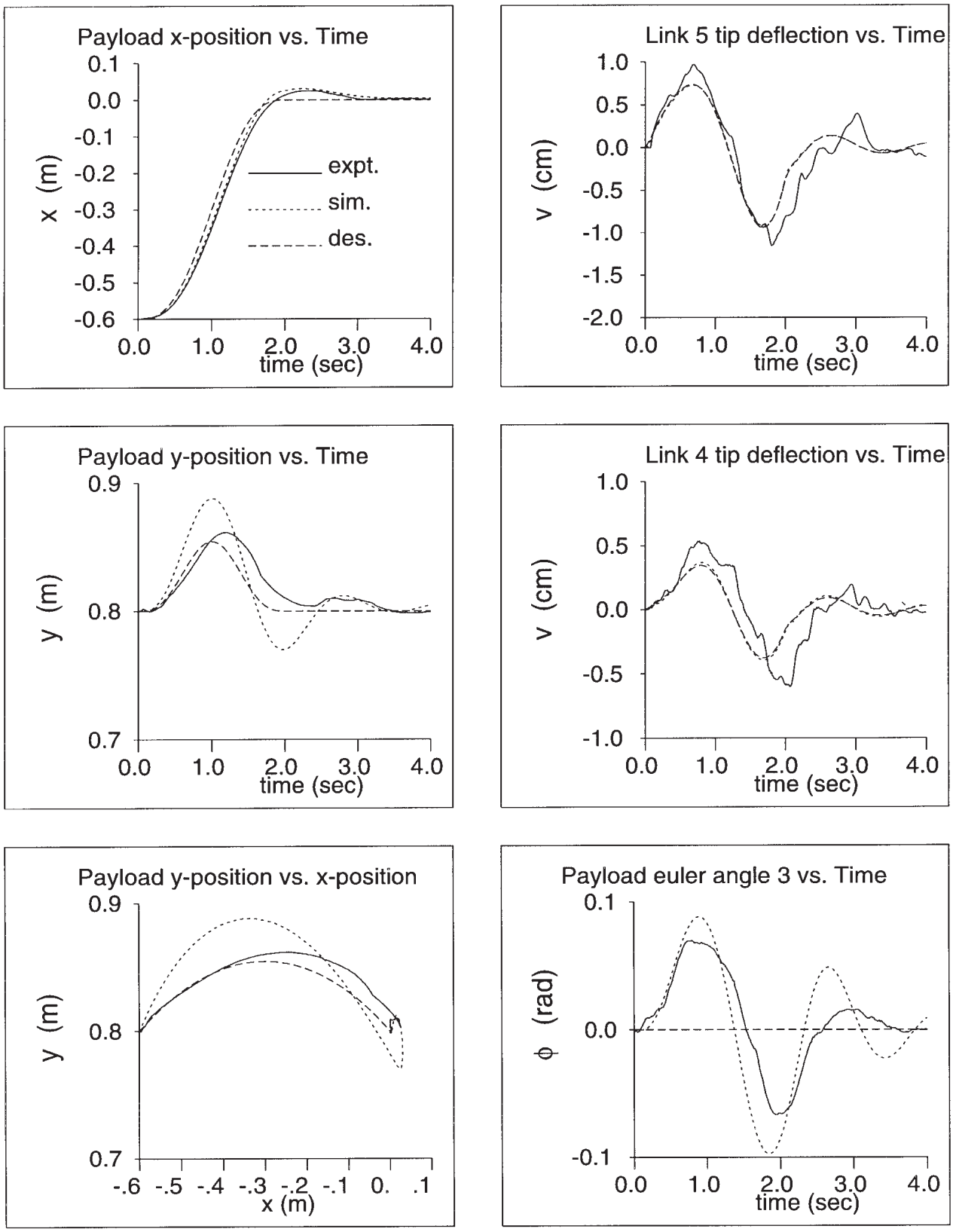


Fig. 11. Results for $x$-translation ($C_1 = 0.75$, $C_2 = 0.25$).

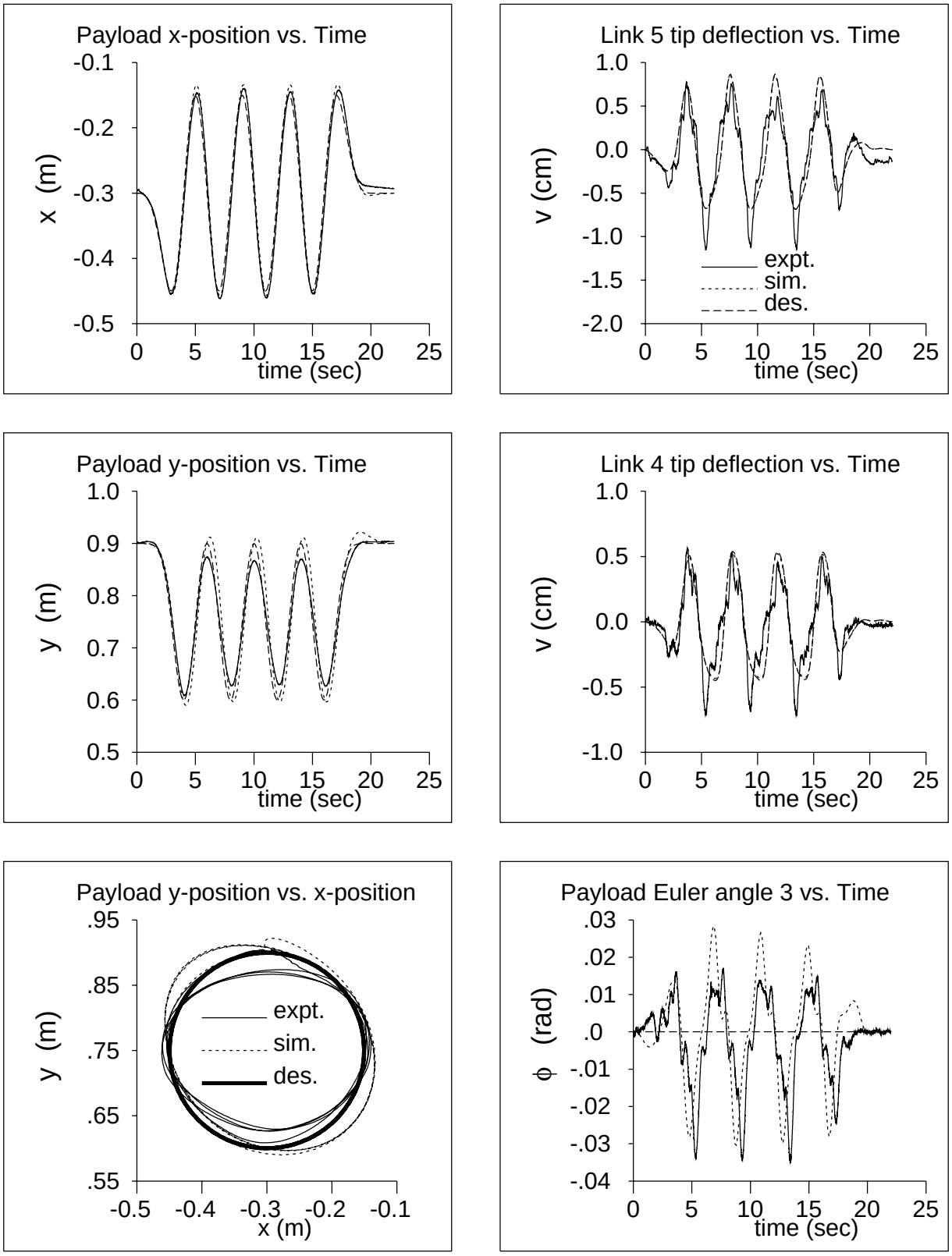


Fig. 12. Results for circle trajectory ($C_1 = 0.5$, $C_2 = 0.5$).

## References


Bonaventura, C. S., and Lilly, K. W. 1995. A constrained motion algorithm for the shuttle remote manipulator system. *IEEE Control Systems Magazine* 15(5):6–16.

Book, W. J. 1993. Structural flexibility of motion systems in the space environment. *IEEE Trans. on Robotics and Automation* 9(5):524–530.

Canudas de Wit, C., Siciliano, B., and Bastin, G., eds. 1996. *Theory of Robot Control*. London: Springer-Verlag.

Damaren, C. J. 1995. Passivity analysis for flexible multilink space manipulators. *AIAA J. of Guidance, Control, and Dynamics* 18(2):272–279.

Damaren, C. J. 1996a. Approximate inverse dynamics and passive feedback for flexible manipulators with large payloads. *IEEE Trans. on Robotics and Automation* 12(1):131–138.

Damaren, C. J. 1996b. Adaptive control of flexible manipulators carrying large uncertain payloads. *J. of Robotic Systems* 13(4):219–228.

Damaren, C. J. 1998. Modal properties and control system design for two-link flexible manipulators. *Int. J. Robotics Research* 17(6):667–678.

Damaren, C. J., and D'Eleuterio, G.M.T. 1989. On the relationship between discrete-time optimal control and elastic multibody dynamics. In *Contemporary Mathematics*, Vol. 97, ed. J. E. Marsden, P. S. Krishnaprasad, and J. C. Simo. Providence, RI: American Mathematical Society.

Damaren, C. J., and Sharf, I. 1995. Simulation of flexible-link manipulators with inertial and geometric nonlinearities. *ASME J. of Dynamic Systems, Measurement, and Control* 117(1):74–87.

Garcia de Jalon, J., and Bayo, E. 1994. *Kinematic and Dynamic Simulation of Multibody Systems: The Real-Time Challenge*. New York: Springer-Verlag.

Hu, F. L., and Ulsoy, A. G. 1994. Dynamic modeling of constrained flexible robot arms for controller design. *ASME J. of Dynamic Systems, Measurement, and Control* 114:56–65.

Krishnamurthy, K., and Yang, L. 1995. Dynamic modeling and simulation of two cooperating structurally-flexible robotic manipulators. *Robotica* 13:375–384.

Lilly, K. W., and Orin, D. E. 1991. Efficient dynamic simulation of a single closed-chain manipulator. *Proc. of IEEE Int. Conference on Robotics and Automation*, Sacramento, April, pp. 210–215.

Nakamura, Y., and Ghodoussi, M. 1989. Dynamics computation of closed-link robot mechanisms with nonredundant and redundant actuators. *IEEE Trans. on Robotics and Automation* 5(3):294–302.

Newcomb, R. W. 1966. *Linear Multiport Synthesis*. New York: McGraw-Hill.

Ortega, R., Loría, A., Nicklasson, P. J., and Sira-Ramírez, H. 1998. *Passivity-Based Control of Euler-Lagrange Systems*. London: Springer-Verlag.

Uchiyama, M. 1998. Multi-arm robot systems. In *Complex Robotic Systems*, ed. P. Chiacchio and P. Chiaverini. London: Springer-Verlag.

Uecker, D. R., Wang, Y., and Kokkinis, T. 1991. Experimental evaluation of real-time model-based control of a 3-dof closed-chain direct-drive mechanism. *Proc. of IEEE Int. Conference on Robotics and Automation*, Sacramento, April, pp. 1861–1866.

Unseren, M. A. 1998. Load distribution and control of interacting manipulators. In *Complex Robotic Systems*, ed. P. Chiacchio and P. Chiaverini. London: Springer-Verlag.

Wang, D., and Vidyasagar, M. 1990. Passive control of a single flexible link. *Proc. of IEEE Int. Conference on Robotics and Automation*, Vol. 2, Cincinnati, April, pp. 1432–1437.

Wang, D., and Vidyasagar, M. 1991. Transfer functions for a single flexible link. *Int. J. Robotics Research* 10(5):540–549.

Yim, W., and Singh, S. N. 1995. Inverse force and motion control of constrained elastic robots. *ASME J. of Dynamic Systems, Measurement, and Control* 117(3):374–383.